JAMES | Journal of Advances in Modeling Earth Systems

RESEARCH ARTICLE
10.1029/2024MS004630

The Rapid Transition From Shallow to Precipitating Convection as a Predator–Prey Process

Cristian V. Vraciu[1,2], Julien Savre[3], and Maxime Colin[4]

[1]Faculty of Physics, University of Bucharest, Bucharest–Măgurele, Romania, [2]Department of Theoretical Physics, Horia Hulubei National Institute of Physics and Nuclear Engineering, Măgurele, Romania, [3]Meteorology Institute, Ludwig-Maximilians-Universität München, Munich, Germany, [4]Leibniz Centre for Tropical Marine Research, Bremen, Germany

Key Points:

- A conceptual picture for cumulus cloud populations based on cloud–updraft interaction is discussed
- The local shallow preconditioning and the cold pool feedback imply a predator–prey type of interaction in the cloud–precipitation system
- A simple predator–prey model shows good agreement with idealized numerical simulations for the rapid shallow–to–deep transition

Correspondence to:
C. V. Vraciu,
cv.vraciu@gmail.com

Citation:
Vraciu, C. V., Savre, J., & Colin, M. (2025). The rapid transition from shallow to precipitating convection as a predator–prey process. *Journal of Advances in Modeling Earth Systems*, *17*, e2024MS004630. https://doi.org/10.1029/2024MS004630

Received 10 AUG 2024
Accepted 6 JAN 2025

Author Contributions:
Conceptualization: Cristian V. Vraciu, Maxime Colin
Formal analysis: Cristian V. Vraciu
Investigation: Cristian V. Vraciu, Julien Savre
Methodology: Cristian V. Vraciu, Julien Savre
Visualization: Cristian V. Vraciu
Writing – original draft: Cristian V. Vraciu
Writing – review & editing: Cristian V. Vraciu, Julien Savre, Maxime Colin

Abstract Properly predicting the rapid transition from shallow to precipitating atmospheric convection within a diurnal cycle over land is of great importance for both weather prediction and climate projections. In this work, we consider that a cumulus cloud is formed due to the transport of water mass by multiple updrafts during its lifetime. Cumulus clouds then locally create favorable conditions for the subsequent convective updrafts to reach higher altitudes, leading to deeper precipitating convection. This mechanism is amplified by the cold pools formed by the evaporation of precipitation in the sub-cloud layer. Based on this conceptual view of cloud–cloud interactions which goes beyond the one cloud equals one–plume picture, it is argued that precipitating clouds may act as predators that prey on the total cloud population, such that the rapid shallow–to–deep transition can be modeled as a simple predator–prey system. This conceptual model is validated by comparing solutions of the Lotka-Volterra system of equations to results obtained using a high-resolution large-eddy simulation model. Moreover, we argue that the complete diurnal cycle of deep convection can be seen as a predator–prey system with varying food supply for the prey. Finally, we suggest that based on the present conceptual model, new unified cloud-convection parameterizations can be designed which may lead to improved representations of the transition from shallow to precipitating continental convection.

Plain Language Summary The rapid transition from shallow to precipitating convection over land is still poorly represented by weather and climate models. In this work, we argue that this is due to the fact that the convective parameterization schemes only consider the interaction between the clouds and their environment, which is a slow process, and do not consider cloud–cloud interactions during the transition, which is a fast process. We show that this latter interaction can be modeled as a predator–prey process, and we show how a very simple dynamical model for cloud population can lead to improved prediction for the precipitation rate and cloud cover over land.

1. Introduction

Atmospheric convection transports heat and moisture from the surface throughout the troposphere creating cumulus and cumulonimbus clouds that are responsible for the water cycle in the atmosphere and have a strong radiative effect that can lead to either warming or cooling of the atmosphere. Shallow cumulus clouds are non–precipitating, or weekly precipitating convective clouds that form when the convective updrafts from the boundary layer reach the lifting condensation level but are unable to reach higher altitudes as they lose their buoyancy very quickly. Predicting shallow clouds is important for climate predictability as they cover a large part of the Earth and they reflect an important fraction of the solar radiation back into space so that they have a strong cooling effect on the climate system. When the atmosphere is unstable and the convective updrafts are able to reach the level of free convection (LFC), deep, precipitating convection is initiated. The deep convective clouds (congestus and cumulonimbus) precipitate, and re–stabilize the atmosphere as they warm and dry their environment. Since the cumulonimbus clouds are responsible for the formation of cirrus clouds, they also play an important role in controlling the radiative budget of the Earth, as the cirrus clouds have a net warming effect. Therefore, the manner shallow and deep convective clouds are represented in climate models has a significant impact on climate predictions.

In general, the presence of a convective inhibition (CIN) layer prevents boundary layer updrafts from spontaneously reaching their LFC and slows down the development of deep precipitating clouds: in this situation, shallow cumuli develop first and contribute to the creation of conditions favorable to deep convection. The

transition from shallow to precipitating convection can be considered of two types: (a) a slow transition when at the beginning the atmosphere is not unstable enough to sustain the development of precipitating convection, and the shallow cumuli slowly moisten the atmosphere until the environment is unstable enough to allow the clouds to grow deeper and precipitate (Champouillon et al., 2023; Yano & Plant, 2012b), which is a process that takes typically a few days; (b) a rapid transition in which the atmosphere is already unstable but deep precipitating convection still takes a few hours to develop. This rapid transition usually occurs over the tropics where the atmosphere is always unstable (Hohenegger & Stevens, 2013). In a diurnal cycle over land, the rapid transition has been documented by several authors (Grabowski, 2023; Grabowski et al., 2006; Khairoutdinov & Randall, 2006; Kurowski et al., 2018; Savre & Craig, 2023). In this particular case, the transition starts when the CIN becomes small, and it takes around 3–4 hr for precipitation to properly develop, despite having a very large convective available potential energy (CAPE) from the beginning. In this study, we focus on the second kind of shallow–to–deep transition.

Although in recent years many studies investigated the physical processes controlling the rapid transition from shallow to precipitating convection (Kurowski et al., 2018; Peters et al., 2022; Powell, 2022; Rochetin et al., 2014; Schiro & Neelin, 2019), weather and climate models still predict the onset of deep precipitating convection to occur around 2–5 hr earlier when compared to observations (Christopoulos & Schneider, 2021; Song et al., 2024) or large–eddy simulation (LES) (Bechtold et al., 2004; Couvreux et al., 2015; Grabowski et al., 2006; Harvey et al., 2022; Tao et al., 2023) within a diurnal cycle over land. That is because the convective parameterization schemes immediately switch to deep convection when CIN is very small and CAPE is large, although in reality, even when these conditions are met, the transition still takes a few hours (an effect which is called convective memory), or may not even occur within a diurnal cycle (Khairoutdinov & Randall, 2006; Nelson et al., 2021; Tian et al., 2021; Zhuang et al., 2017).

The majority of convective parameterization schemes used in climate models are based on the so–called mass–flux parameterization. The objective of these parameterizations is to find the mass flux of the clouds and to provide feedback to the large–scale resolved by the model. The mass–flux formulation separates closure, triggering, and plume model. It is based on the idea that the clouds, or the whole ensemble of clouds, can be modeled as steady–state plumes. In the picture used by these formulations, a convective cloud is formed by only one entraining plume, which only entrains environmental air described by the mean resolved state (Arakawa, 2004; Plant, 2010; Yano, 2014). Thus, the mass flux is estimated in these parameterization schemes only by considering the large–scale state, neglecting any cloud–cloud interaction or heterogeneity within a given grid box. As the mass flux only changes with the slow change of the large–scale state, these schemes are unable to catch any rapid transition from shallow to precipitating convection (Bechtold et al., 2004). At the time Arakawa and Schubert (1974) formulated their parameterization, the grid box and the time–stepping used by climate models were so large that over the tropical ocean one could consider that at all times within a grid–box there is a spectrum of shallow and precipitating clouds that are in quasi–equilibrium with their environment. Many operational parameterization schemes still follow the original mass–flux formulation introduced by Arakawa and Schubert (1974) (e.g., Bechtold et al., 2014; Kain & Fritsch, 1993; Rio et al., 2019). However, nowadays, climate models have much finer resolutions, both in space and time, and the quasi–equilibrium is therefore not satisfied in every grid box at every time step (Davies et al., 2013; Donner & Phillips, 2003; Jones & Randall, 2011). To improve the representation of atmospheric convection in numerical models with high temporal resolution, several prognostic closures for the convective mass flux with relaxed quasi–equilibrium have later been formulated (e.g., Moorthi & Suarez, 1992; Pan & Randall, 1998; Wagner & Graf, 2010; Yano & Plant, 2012a).

In general, the time evolution of the convective mass flux at cloud base M_c, where $M_c = \rho_0 \sigma_c w_c$, can be written as:

$$\frac{dM_c}{dt} = \rho_0 \sigma_c \frac{dw_c}{dt} + \rho_0 w_c \frac{d\sigma_c}{dt}, \tag{1}$$

where t is the time, ρ_0 is the atmospheric density at the cloud base, σ_c is the convective cloud cover, and w_c is the convective updraft velocity of the convective clouds. The mass-flux parameterizations usually consider that σ_c is constant, and thus, only the first term on the right-hand side (rhs) of Equation 1 is important. Although the traditional mass–flux formulations do not make the assumption that σ_c is constant in an explicit way, such an assumption can be easily justified if the grid box and the time step are very large, such that the fluctuations in σ_c

are subgrid, and the increase in cloud population in a small subdomain is compensated by the decay of clouds in another small subdomain. Therefore, in the mass–flux parameterization schemes, the triggering of individual convective clouds is not considered, but rather the whole spectrum of clouds that slowly interacts with the large–scale environment (Yano et al., 2013). It should also be noted that parameterization models that implement a momentum equation for w_c in which the assumption that σ_c is constant is made in an explicit way have been formulated (e.g., Bechtold et al., 2001; Bretherton et al., 2004; Donner, 1993). This approach is also considered by the so-called eddy-diffusivity mass-flux formulations, which represent the local turbulent mixing with an eddy-diffusivity closure, and the non-local convective transport by a mass-flux approach, in which the mass flux is generally modeled by solving a plume model for the updraft velocity w_u, while σ_c is usually assumed constant (Hourdin et al., 2002; Siebesma et al., 2007; Teixeira et al., 2023; Vraciu, 2024). As in the original mass–flux formulation based on quasi–equilibrium, the prognostic formulations of Pan and Randall (1998) also consider a constant σ_c, and a plume that only interacts with a homogeneous environment. Conversely, Yano and Plant (2012a, 2012b) assume that the time evolution of the mass flux is only controlled by the convective cloud cover, but it also considers the steady–state plume model while completely neglecting any cloud–cloud interaction.

Within a diurnal cycle over land, however, if the atmosphere is already unstable in the morning, the convection develops quite rapidly, while the cloud environment remains rather steady during the day (Tian et al., 2021). In such cases, one can no longer assume that the convection only interacts with the environment, and thus, convective memory might be important (Colin & Sherwood, 2021; Colin et al., 2019; Daleu et al., 2020; Hwong et al., 2023). Although the above mentioned prognostic formulations also introduce convective memory into their formulation, this is achieved based on somewhat *ad-hoc* relations, and not fully based on physical considerations. The main assumption in these prognostic formulations is that M_c does not respond immediately to changes in the large–scale state. However, it is not clear why such an assumption about the closure might be true for a steady–state plume model that only interacts with a homogeneous environment. In the present work, we note that the updraft velocity at cloud base only exhibits a slow change during the rapid shallow–to–deep transition over land (e.g., Figure 15 of Kurowski et al. (2018)), whereas the cloud fraction of the precipitating clouds evolves from zero in the morning to a maximum around noon, and thus, for this particular case, the second term in the rhs of Equation 1 becomes significant (as for Yano and Plant (2012a, 2012b)). Thus, the scope of this study is to find a dynamical system able to represent the evolution of σ_c during the rapid transition from shallow to precipitating convection, provided the updraft velocity at cloud base can be considered constant.

There is a special family of models for convection and clouds based on the predator-prey concept that relates to this study. Nober and Graf (2005) introduced a promising spectral model for convection in which the various cloud types are competing for atmospheric instability according to a Lotka–Volterra predator-prey model. This spectral approach reminds us of the classical model by Arakawa and Schubert (1974), but in addition relaxes the quasi-equilibrium assumption. This model allows for cloud-cloud interactions, but unfortunately, in an indirect way, through the impact of each cloud on the mean profiles. Wagner and Graf (2010) extended the previous Lotka-Volterra model to incorporate a cloud model with entrainment for the cloud populations, and proposed a derivation following Pan and Randall (1998), which has been contested by Plant and Yano (2011). In the model by Koren and Feingold (2011) and Feingold et al. (2015) for stratocumulus clouds, rain acts as a predator on clouds, and the interaction is mediated by aerosol concentration. This model has the advantage of having an explicit time delay in the equations, but it is not tailored for deep convection. Colin and Sherwood (2021) also formulate a Lotka–Volterra model, in which convection and the small-scale convective heterogeneity (such as cold pools and updrafts) prey upon large-scale atmospheric instability, which creates a delay and memory in convective development. Their equations end up similar to those in the discharge-recharge cycle by Yano and Plant (2012a), and some concepts are connected to Nober and Graf (2005). Their model manages to capture the behavior of idealized perturbation experiments, and relates to the idea of a memory based on thermodynamic structures. Neggers and Griewank (2021) proposed a framework to introduce convective cloud population dynamics into models, and in particular, they have tested a predator-prey interaction. Their framework is appealing, but it is not directly applied to the type of cloud-cloud interactions we focus on here.

The advantage of predator-prey models is that they borrow from population dynamics, they can easily include convective memory in time and interactions in space, and they are a bottom-up approach for cloud growth. The downside is that they are simplified models, and tuning the parameters of such models can be a challenge, although it can be done successfully for given purposes (Lunderman et al., 2020). There is an interesting

exception with Nober and Graf (2005) in which no tuning is required since the parameters are computed by the model itself, however in this case the model could be very sensitive to initial conditions. Here, we will also introduce a simple predator-prey model of convection. But unlike most previous models (the exception being Neggers and Griewank (2021)), in our simple predator-prey model, the prey and the predator are both the clouds themselves: the deeper clouds are consuming the cloud field (as with cannibalism). This way, cloud growth does not depend on the large-scale state (which imposes only slowly-varying conditions here), but on the small-scale interactions between clouds (more precisely, the interactions between the updraft population), which is exactly the overlooked element to model properly in conceptual pictures and in parameterizations.

In this work, we first propose a conceptual model for cumulus clouds that allows for a gradual deepening of precipitating convection within a diurnal cycle. Our conceptual model is based on recent evidence that shows that, within a cumulus, multiple updrafts can develop, which allows for local moisture preconditioning. Moreover, the role of the cold pools in the shallow–to–precipitating transition is reviewed here. Contrary to the picture that the cold pools promote deepening due to an increase in the updrafts width (e.g., Schlemmer & Hohenegger, 2014), in our conceptual model, the deepening is promoted due to the organization of updrafts in the sub–cloud layer, which also explains the reduction of the total cloud cover induced by the cold pools. Second, we suggest that in our conceptual model, the interaction between the total cloud field and the precipitating cloud field is similar to a predator–prey interaction in a biological system, and show that, indeed, the total and the precipitating cloud fields in a diurnal cycle of deep convection can follow a Lotka–Volterra type of interaction in idealized large–eddy simulations. The potential role of our conceptual model in convective parameterization schemes with convective memory is also discussed at the end of this work.

2. Conceptual Model

In our model, the clouds are formed due to the transport of water by the updrafts from the boundary layer. In contrast with the mass–flux formulation, we do not consider that every cloud, or every cloud ensemble, is described by only one steady–state plume, but we consider that a cloud can be formed by the contribution of multiple unsteady convective elements — such as thermals (e.g., Hernandez-Deckers & Sherwood, 2016; Scorer & Ludlam, 1953; Sherwood et al., 2013) or starting plumes (Pinsky et al., 2022) or other bubble-like elements (e.g., Malkus & Scorer, 1955; Morrison et al., 2020; Moser & Lasher-Trapp, 2017; Vraciu et al., 2023). Indeed, the pulsating behavior of clouds has been documented by both observational studies (e.g., Damiani et al., 2006; Harrington, 1958; Koenig, 1963; Raymond & Blyth, 1989) and numerical simulations (e.g., Heus et al., 2009; Peters et al., 2019; Sakradzija et al., 2015; Zhao & Austin, 2005), which may indicate the presence of successive convective elements within the clouds. Each convective element transports a finite mass of water from the boundary layer to the cloud layer, and the cloud dimension is given by the total amount of water transported by the set of convective elements that reach the condensation level in that given place of the cloud during its lifetime, minus the amount of cloud water that evaporates due to mixing with the environment (detrainment). The episodic mixing model of Emanuel (1991) is in fact based on a very similar conceptual picture (see also Emanuel, 1993). Emanuel (1991) makes very clear that in his parameterization scheme, the small convective elements within the clouds are responsible for the convective transport: "I am explicitly attempting to represent the collective effects of an ensemble of individual, $\mathcal{O}$(100 m)–scale drafts, not of ensembles of $\mathcal{O}$(1 km)–scale clouds. These drafts, rather than whole clouds, are regarded as the fundamental agents of convective transport." In this picture, a cloud can be seen as analogous to a wall of bricks, and a convective element as a new brick fixed on the wall by the builder — the clouds are seen as a collection of water elements brought by a number of convective elements during the cloud lifetime, in which every water element represents a brick in our wall. This building process can be visualized for the development of a real cumulonimbus cloud at Kjoenbongarit (2013) or for a congestus cloud at Strong (2017).

We consider here two types of clouds: (a) shallow nonprecipitating cumuli, which are those clouds with a top close to the boundary layer depth, covering a fraction σ_s—this type of clouds remain shallow as they are unable to gain buoyancy, or lose their buoyancy very quickly; and (b) convective precipitating clouds, which are clouds that are able to gain some buoyancy and have a top much deeper than the boundary layer depth, covering a fraction σ_c. For simplicity, we consider here as convective precipitating clouds those that have a top above 4 km. Therefore, the total cloud cover is $\sigma = \sigma_s + \sigma_c$. The difference between the shallow and convective precipitating clouds is that the shallow clouds decay only due to mixing (detrainment) into the environment, whereas the convective precipitating clouds decay also by precipitation. Although the shallow cumuli can also lightly precipitate, we

assume that the precipitation rate of shallow cumuli can be neglected with respect to the precipitation rate of convective precipitating clouds.

We consider that the total mass m_j of cloud j is given by:

$$m_j = \sum_i^n \delta m_{j,i} - m_{D,j}, \tag{2}$$

where $\delta m_{j,i}$ is the mass transported into the cloud j by the convective element i, n is the total number of convective elements that contribute to cloud j during its lifetime, and $m_{D,j}$ is the mass lost by the cloud due to mixing with the dry environment and precipitation. Here, by cloud mass, we refer to the mass of air within a cloud, but other quantities might be considered as well, such as the mass of condensed particles (water plus ice), or the total integrated condensed water path. For the whole ensemble of clouds we can write:

$$m = \sum_j m_j = \overline{\rho}\sigma\overline{\Delta z}, \tag{3}$$

where m and $\overline{\Delta z}$ are the total mass and the average depth of the cloud ensemble, respectively, and $\overline{\rho}$ is the mean air density within the clouds. Here, all masses are per unit of area, so the masses in Equation 2 have units of kg m^{-2}. For the evolution of m, neglecting the time change of $\overline{\rho}$, we thus have:

$$\frac{dm}{dt} = \overline{\rho}\sigma\frac{d\overline{\Delta z}}{dt} + \overline{\rho}\,\overline{\Delta z}\frac{d\sigma}{dt} = M_0 - D, \tag{4}$$

where M_0 is the sum of the contributions from all convective elements to the total mass flux at the condensation level and $D = d\left(\sum_j m_{D,j}\right)/dt$, is the rate at which the cloud ensemble loses mass due to evaporation and precipitation. Therefore, the evolution of the cloud fraction becomes:

$$\frac{d\sigma}{dt} = \frac{M_0 - D}{\overline{\rho}\overline{\Delta z}} - \sigma\frac{d\left(\ln\overline{\Delta z}\right)}{dt}. \tag{5}$$

For a shallow case at equilibrium, $M_0 - D = 0$, meaning that the new mass brought into the cloud layer by the convective elements is compensated by the detrainment into the environment. However, during the shallow–to–deep transition, $\overline{\Delta z}$ increases rapidly, and the second term in the rhs of Equation 5 is positive and contributes to a reduction of the total cloud cover. It should be noted that, during the transition, $M_0 - D$ may not be constant as for a shallow case at equilibrium. However, it is clear that since the first term on the rhs is inversely proportional to $\overline{\Delta z}$, the contribution from $M_0 - D$ to the evolution of σ will decrease as the cloud layer depth increases. In any case, as is going to be seen, M_0 decreases during the transition, being correlated with σ, and thus, according to Equation 5, the cloud cover further decreases. Equation 5 thus indicates that the mass conservation implies a reduction in the total cloud fraction during the rapid shallow–to–deep transition.

2.1. Local Moisture Preconditioning

Because the moisture of the cloud environmental layer has been observed to be an important factor in the transition from shallow to precipitating convection, some studies argue that the rapid transition from shallow to precipitating convection can be explained by the moistening of the cloud environment by the shallow cumuli (Holloway & Neelin, 2009; Waite & Khouider, 2010), which is known as the moisture preconditioning mechanism. This idea can be perhaps better understood if we consider the following plume model (Morrison, 2017):

$$\frac{dB}{dz} = -N^2 - \varepsilon B - \varepsilon\frac{gL_v q_{sE}(1 - \mathcal{R}_E)}{c_p T_E \Gamma}, \tag{6}$$

where B is the plume buoyancy, z is the vertical coordinate, N^2 is the squared buoyancy frequency, ε is the entrainment rate, g is the gravitational acceleration, L_v is the latent heat of vapourization, q_{sE} is the saturation

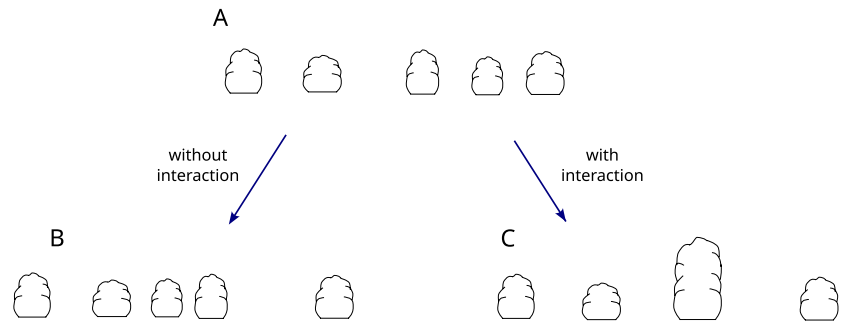

Figure 1. Deepening of a cumulus clouds due to local preconditioning. (a) Initial cloud field with five shallow cumuli. (b) After a time, one of the clouds decays, while a new set of convective elements, that do not interact with the existing clouds, forms a new shallow cumulus. As a result, the cloud fraction remains steady. (c) As in (b), but now the new set of convective elements develop in the place of one of the existing clouds, forming a deeper, convective precipitating cloud. As a result, the cloud fraction at cloud base decreases, while the cloud fraction of convective precipitating cumuli increases.

mixing ratio of the environment, $\mathcal{R}_E$ is the environmental relative humidity, T_E is the temperature of the environment, c_p is the specific heat of air at constant pressure, and $\Gamma \approx 1 + L_v^2 q_{sE}/\left(c_p R_v T_E^2\right)$ is a parameter, for which R_v is the water vapor gas constant. The last term in the rhs of Equation 6 represents the cooling rate of the updraft plume due to the evaporation of the cloud water that mixes with the dry environmental air. Thus, as shallow cumuli continue to increase $\mathcal{R}_E$, this term will continue to decrease, allowing the plumes to deepen the cloud layer (Morrison et al., 2022). However, Hohenegger and Stevens (2013) showed that the moisture preconditioning acts at time scales too long to explain the rapid transition. Note that the concept of preconditioning as formulated by Waite and Khouider (2010) or Yano and Plant (2012b) is based on the same consideration as the mass–flux formulation, with steady plumes that entrains air described by a mean domain value.

On the other hand, Vraciu et al. (2023) discussed the role of passive shallow cumuli in the transition from shallow to deep convection, which can be regarded as local moisture preconditioning. As in the moisture preconditioning mechanism described by (e.g., Waite & Khouider, 2010), the idea is that if the updraft plumes can entrain moister air, they will be able to grow deeper due to a smaller contribution of the last term in the rhs of Equation 6. However, the main difference is that we no longer assume a steady–state plume that entrains air only described by a mean state, as in the mass–flux formulation, but we consider that the plumes (or any other convective elements) have a smaller lifetime than the clouds, and are allowed to develop in the place of existing clouds. Thus, the cloud itself provides a local preconditioning for the development of the subsequent convective elements, as also shown by Moser and Lasher-Trapp (2017). This process of interaction between the convective elements and the existing clouds leads to deeper and deeper clouds. Furthermore, we can also consider that the clouds, even after a complete decay, still leave spots of abnormally large humidity that slowly dissipate into the environment (e.g., Figure 7 of Daleu et al. (2020)). Thus, if the convective elements reach the condensation level in the location of such spots, they will again benefit from local preconditioning, creating deeper clouds. We may also consider that the area of these spots is proportional to the total cloud cover at the cloud base.

Let us consider that at a given time we have a cloud field of shallow cumuli, as schematically presented in Figure 1a. We consider that every cloud, either shallow or deep, is formed by a set of convective elements that transported water from the boundary layer to the cloud layer. After a given time, a new set of convective elements reaches the condensation level. Here, we have two possibilities: (a) the convective elements reach the condensation level in a place where there is no cloud (or spots of large humidity), forming new shallow cumuli. This case is schematically illustrated in Figure 1b. At the same time, some of the clouds decay during the development of the new convective elements, and thus, we can consider that the new clouds statistically replace the old ones that died; (b) the new set of convective elements reach the condensation level in the place of an already existing cloud, as schematically illustrated in Figure 1c. In this case, the convective elements will transport water from the boundary layer in a higher cloud layer, while some of the shallow clouds decay. As a result, the total cloud fraction σ decreases, while the fraction of clouds that become convective σ_c increases.

As convection becomes more intense, the compensating entrainment of dry air from the cloud layer into the boundary layer also increases, which creates a stable transition layer between the top of the boundary layer z_i and

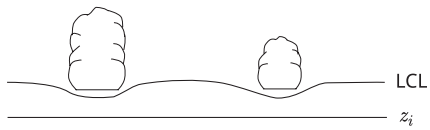

Figure 2. Schematics of non–precipitating clouds altering the transition layer between z_i and LCL.

the lifting condensation level (LCL) (Albright et al., 2022; Betts, 1976; Neggers et al., 2006). As a result, the mass flux of the updrafts at cloud base may also decrease as the number of convective precipitating clouds increases. Because the non–precipitating clouds always mix with the environment due to diffusion and turbulent mixing, we expect the air just below the base of a given non–precipitating cloud to be moister than the air at the same height but in a cloudless area (e.g., Albright et al., 2023). Thus, as the convective elements that develop in the place of an already existing cloud mix moister air than those developing in the cloudless areas, we consider that the non–precipitating clouds also create heterogeneity in the stable transition layer (Figure 2), making easier for the convective elements to reach the condensation level where non–precipitating clouds are already present. This alteration of the transition layer is also supported by the findings of Vraciu et al. (2023) who showed that the fraction of convective elements that develop where a cloud is already present is comparable with the fraction of convective elements that develop in cloudless areas, even though the clouds only occupy a very small fractional area. Therefore, we expect the fraction of updrafts at the cloud base to also decrease with the decrease of σ, which leads to a further reduction in σ. The local shallow preconditioning thus leads to deeper clouds, which due to mass conservation and alteration of the transition layer leads to a reduction in the cloud cover at cloud base.

2.2. Cold Pools Feedback

Once the clouds begin to precipitate, cold pools are formed in the boundary layer, which organize the convective field. This organization can be seen as updrafts being larger and more organized (Meyer & Haerter, 2020; Schlemmer & Hohenegger, 2014). This leads to further deepening of the cloud layer for two reasons: first, the larger convective elements experience smaller entrainment (Kurowski et al., 2018; Schlemmer & Hohenegger, 2014), and thus, are able to better preserve their buoyancy, and second, more organized convective elements facilitate the local preconditioning, as the probability for a set of convective elements to develop in a certain place (to cluster) is larger. Although one may argue that the cold pools lead to convective elements that are so large that they do not require local preconditioning, Savre and Craig (2023) show that, during the transition, the increase in the updraft dimension is negligible compared with the increase in cloud dimension, as also suggested by Kurowski et al. (2024)—there is no updraft as large as a deep convective cloud, and thus, we argue here that cold pools essentially make the local preconditioning more efficient without substantially altering the properties of the boundary layer updrafts. In other words, we still consider that a convective cloud is a result of multiple convective elements bringing water from the boundary layer in the same location, but since the convective elements are larger and better organized, a smaller number of convective elements are required to build a precipitating cloud. Following the analogy between clouds and brick walls, we can picture the cold pool feedback as having sets of bricks that are already tied together, and thus, the building process is much more efficient since the builder brings a new set of tied bricks with only one move. Although we do not consider that it is impossible for only one convective element to create a precipitating cloud, we consider that even in this case, the convective element will benefit from the large humidity spots created by the non–precipitating clouds, and such a situation might rather correspond to the creation of "turkey towers"—narrow and deep convective clouds (Figure 3), rather than the creation of congestus or cumulonimbus clouds. The development of such a cloud can be visualized in Herzmann (2017).

In Figure 4, we illustrate the effect of the cold pools in the deepening of subsequent convection. Initially, we consider a field of shallow and precipitating clouds. The precipitating cloud illustrated in Figure 4a precipitates, creating a cold pool, and a new convective precipitating cloud is formed later on, as schematically illustrated in Figure 4b. Since the convective elements are larger and more organized, more water is transported by them to higher altitudes, which leads to a net decrease in the total cloud field. Moreover, although the cold pools trigger new updrafts at their gust fronts (Meyer & Haerter, 2020; Torri et al., 2015), as the cold pools represent areas of evaporatively cooled downdrafts they also inhibit updrafts from developing within these areas. The cold pools thus make the convective elements to be fewer but stronger (e.g., Figure 15 of Kurowski et al. (2018)). Therefore, we also expect a reduction in the updraft fraction at the cloud base due to cold pool feedback.

2.3. Predator-Prey Model

The physical processes discussed above show that convective precipitating clouds grow at the expense of all clouds, due to the preconditioning from all clouds (as if they were replacing shallower clouds). This suggests that

Figure 3. Turkey tower—a deep and narrow cumulus cloud resembling a turkey. Observed over the Carpathian Mountains, Hunedoara County, Romania.

the transition from shallow to precipitating convection can be modeled as a predator-prey process with convective precipitating clouds acting as predators, and the total cloud field acting as prey. We consider that the prey is represented by the total cloud field as both the shallow and convective precipitating clouds precondition their local environment, as long as the convective precipitating clouds are not in the decaying precipitating stage (we can assume that during the rapid shallow–to–precipitating transition, the fraction of clouds in the decaying precipitating stage is much smaller than the total cloud fraction).

Here, for simplicity, we consider a very simple predator–prey model, namely the Lotka–Volterra model (Takeuchi, 1996), given by:

$$\frac{dx}{dt} = ax - bxy, \tag{7}$$

$$\frac{dy}{dt} = exy - fy, \tag{8}$$

where x is the population of prey and y is the population of predators, and a, b, e, and f are system coefficients. A solution of the Lotka–Volterra system is presented in Figure 5.

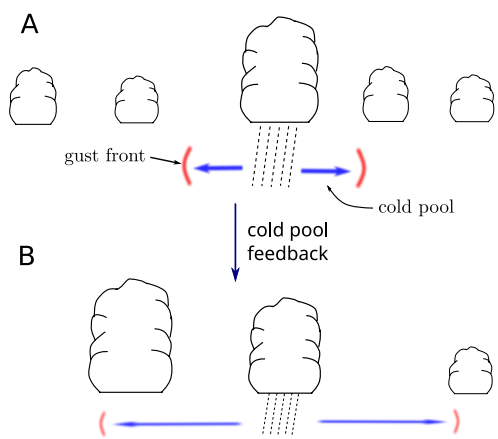

Figure 4. Deepening of a cumulus clouds due to cold pool feedback. (a) Initial cloud field with four shallow clouds and one convective cloud in the decaying precipitating stage, which creates a cold pool that leads to the development of a new convective precipitating cloud at a later time (b). At the same time, some of the shallow clouds decay without being replaced by new shallow cumuli. As the precipitating clouds, being deeper, occupy a smaller fraction than the shallow cumuli, for the same amount of building convective elements, the total cloud cover decreases.

In our case, we consider that the prey is played by the total cloud population at the cloud base, which sustains the development of the deeper clouds, that act as predators. Thus, we consider $x = \sigma$ and $y = \sigma_c$. The Lotka-Volterra model for the total cloud population and precipitating clouds population can be derived by considering a two-layer cloud model, as schematically illustrated in Figure 6. We can write budget equations for the mass of cloud air occupying the first layer, m_1, and for the mass of cloud air occupying the second layer, m_2, as follows:

$$\frac{dm_1}{dt} = M_0 - M_c - D_1, \tag{9}$$

$$\frac{dm_2}{dt} = M_c - D_2, \tag{10}$$

where M_c is the convective mass flux at 4 km altitude, and D_1 and D_2 are the sink rates due to evaporation and precipitation of cloud masses m_1 and m_2, respectively. M_0 and M_c are given by:

$$M_0 = \kappa_1 \overline{\rho_1} w_0 \sigma \quad \text{and} \quad M_c = \kappa_2 \overline{\rho_2} w_c \sigma_c, \tag{11}$$

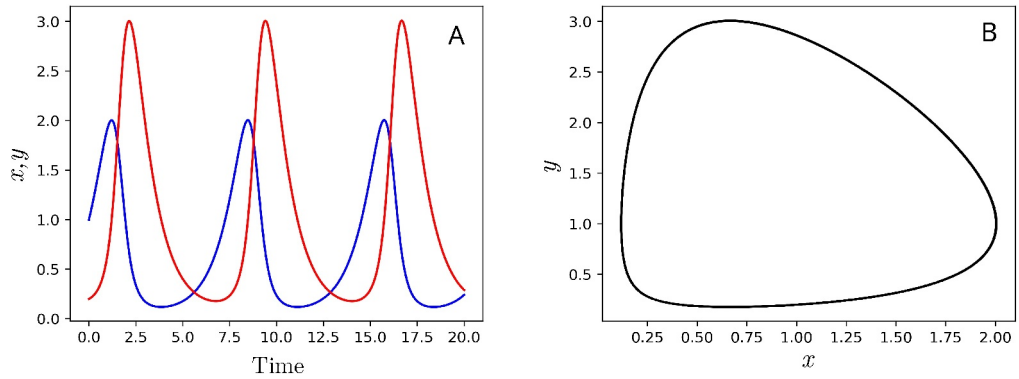

Figure 5. Solution of the Lotka–Volterra system. (a) Time evolution of prey (blue solid line) and predators (red solid line); (b) Limit cycle of the system of the predator–prey system, with x representing the prey and y representing the predators. The cycle goes in anti-clockwise direction.

in which κ_1 and κ_2 are the proportionality coefficients between the updraft cover and the cloud cover at cloud base and 4 km altitude, respectively, and $\overline{\rho_1}$ and $\overline{\rho_2}$ are the mean air densities in the first and second layer, respectively. We thus consider here that the cloud cover and the updraft cover are proportional at a given level. This aspect is tested in Appendix A showing that this is a reasonable assumption during the shallow–to–deep transition. The masses m_1 and m_2 can be expressed as $m_1 = \overline{\rho_1}\sigma\Delta z_1$ and $m_2 = \overline{\rho_2}\sigma_c\Delta z_2$, in which Δz_1 and Δz_2 are the depths of the first and the second layer, respectively. Here, for simplicity, we assume that the clouds occupy the whole space from their base to their respective layer depth, but it can also be considered that they occupy on average a fraction constant in time. We also assume that the sink rates can be parameterized as follows:

$$D_{1,2} = \frac{m_{1,2}}{\tau}(1 - \mathcal{R}_{E1,E2}), \tag{12}$$

where $\mathcal{R}_{E1}$ and $\mathcal{R}_{E2}$ are the environmental relative humidity in the first and in the second layer, respectively, and τ is the cloud lifetime. Thus, the system of Equations 9 and 10 becomes:

$$\frac{d\sigma}{dt} = \left(\frac{\kappa_1 w_0}{\Delta z_1} - \frac{1 - \mathcal{R}_{E1}}{\tau}\right)\sigma - \frac{\kappa_2\overline{\rho_2}w_c}{\overline{\rho_1}\Delta z_1}\sigma_c, \tag{13}$$

$$\frac{d\sigma_c}{dt} = \frac{\kappa_2 w_c}{\Delta z_2}\sigma_c - \frac{1 - \mathcal{R}_{E2}}{\tau}\sigma_c. \tag{14}$$

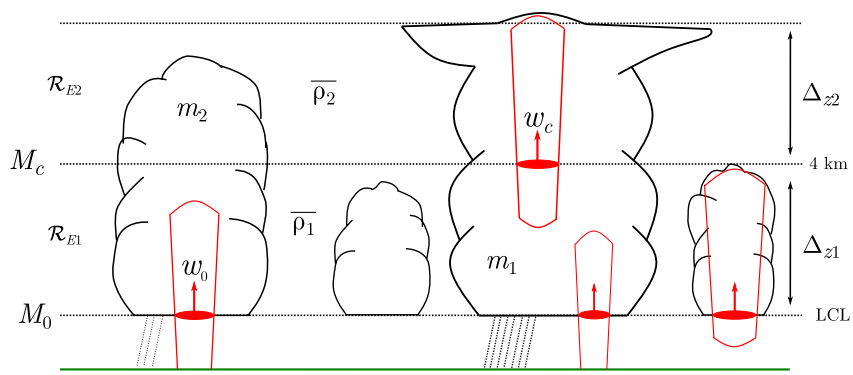

Figure 6. Schematics for a two-layer model of clouds. Clouds that occupy only the first layer between LCL and 4 km altitude are assumed to be non-precipitating shallow cumuli, while the clouds that occupy both layers are assumed to be convective precipitating clouds.

If w_c is proportional to the total cloud cover, then we obtain the Lotka-Volterra model. The updraft velocity w_c can be modeled as follows:

$$w_c = a_0 F(\mathcal{R}_{E1}, \sigma)\sqrt{2CAPE}, \tag{15}$$

where a_0 is a constant and F is a function of $\mathcal{R}_{E1}$ and σ, assumed to represent the local preconditioning. The probability for an updraft to develop within a preexisting cloud can be assumed to be proportional to the total cloud cover σ, and thus, we can consider that $F \propto \sigma$. Thus, as a very simple parameterization, we can consider that F can be parameterized as $F = c\mathcal{R}_{E1}^{\epsilon}\sigma$, in which c is a parameter associated with the cloud-updraft interaction, and ϵ is a positive exponent. We thus expect c to depend on the degree of convective organization. The parameterization of the function F is based on our conceptual model and justified in Appendix B. Therefore, we obtain the Lotka-Volterra system of Equations 7 and 8 with the coefficients a, b, e, f given by:

$$a = \frac{\kappa_1 w_0}{\Delta z_1} - \frac{1 - \mathcal{R}_{E1}}{\tau},$$

$$b = \kappa_2 a_0 c \frac{\overline{\rho_2}\sqrt{2CAPE}}{\overline{\rho_1}\Delta z_1}\mathcal{R}_{E1}^{\epsilon},$$

$$e = \kappa_2 a_0 c \frac{\sqrt{2CAPE}}{\Delta z_2}\mathcal{R}_{E1}^{\epsilon},$$

$$f = \frac{1 - \mathcal{R}_{E2}}{\tau}.$$

The first term in the rhs of Equation 13 represents the difference between the source of new convective elements from the boundary layer and the decay of the old clouds due to the mixing with the environment and precipitation. In the absence of precipitation, all the clouds are shallow. As shallow cumuli moisten their environment, we expect the shallow cloud cover to increase as the lifetime of the clouds increases due to mixing with moister and moister air. Thus, in the absence of precipitation, the shallow cloud cover grows exponentially, which might correspond to a cumulus–to–stratiform transition, rather than the case considered here. The second term represents the decay in the cloud cover due to interactions between precipitating clouds and the rest of the cloud population. Note that this term is associated with the time scale of the shallow to deep transition, with larger values of b representing shorter transition times. Here, the interaction coefficient b is proportional to the lower troposphere relative humidity at the power ϵ and to the squared root of CAPE. Wu et al. (2009) have shown that indeed these two quantities control the transition time. The first term on the rhs of Equation 14 represents the growth of convective precipitating clouds for the same physical arguments as for the second rhs term of the prey equation. Lastly, the last term in the rhs of Equation 14 represents the decay rate of convective precipitating clouds due to precipitation and dissipation into the environment. An important limitation of the Lotka–Volterra model, however, is that predators cannot be created from nothing, and thus, σ_c must be initialized with a nonzero value. Note that the predator–prey system described here comprises cannibalism as the total cloud population, including precipitating clouds, acts as prey for the precipitating cloud population. Although more realistic and accurate predator–prey models may be derived, here we consider the Lotka–Volterra model for its simplicity. Note that we obtained the Lotka–Volterra model by assuming $F \propto \sigma$ in Equation 15, but one may consider for example, that $F \propto \sigma^{\gamma}$, in which γ is a positive parameter. In addition, instead of considering the parameterization for w_c given by Equation 15, one may also model the updraft velocity w_c considering a plume model with cloud–updraft interaction, as proposed by Vraciu et al. (2023), obtaining thus a mass–flux–type of parameterization with cloud–updraft interaction. However, in this work, we only consider the Lotka–Volterra model and leave such a development for future work.

3. Tests and Extensions of the Predator-Prey Model

3.1. LBA Transition Case

Results obtained from a high-resolution large–eddy simulation (LES) were analyzed in order to test our hypotheses. The model configuration constitutes an idealization of the original Large–scale Biosphere–Atmosphere (LBA) case described in Grabowski et al. (2006) with initial conditions and forcings taken from Böing

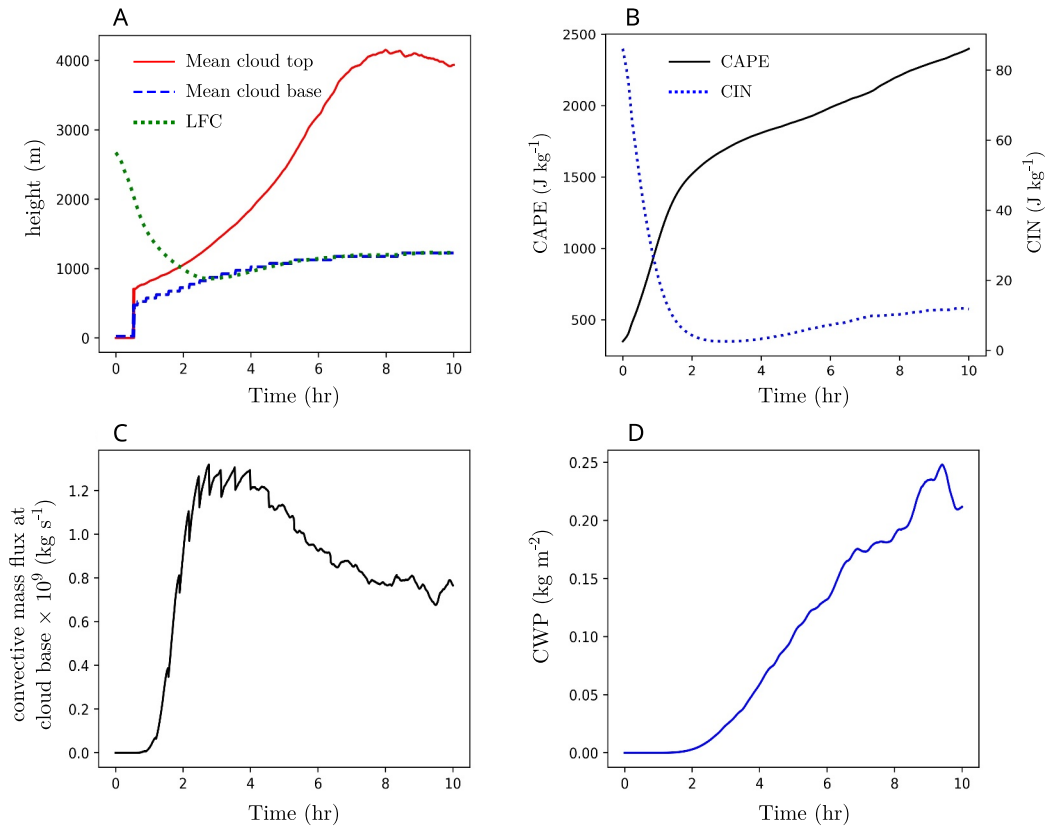

Figure 7. Shallow–to–deep transition in the idealized LBA case. (a) Time series of mean cloud top (red solid line), mean cloud base (blue dashed line), and level of free convection (green dotted line). (b) Time series of convective available potential energy (black solid line) and convective inhibition (blue dotted line). The time series of the convective mass flux at cloud base and of cloud water path are also plotted in (c) and (d), respectively.

et al. (2012). The relative humidity was held constant and equal to 80% up to an altitude of 6,000 m, and then decreased linearly to 15% at 17,500 m. The potential temperature was computed from a prescribed lapse rate following a simple function of altitude, while horizontal winds were initially set to 0 m s^{-1} everywhere. Latent and sensible surface heat fluxes were held constant throughout the simulation and equal to 343 W m^{-2} and 161 W m^{-2} respectively, which corresponds to the diurnal averages of the time-dependent fluxes imposed in Grabowski et al. (2006). Horizontal winds were nudged back to their initial values with a time scale of 6 hr over the course of the simulation, but no other external forcing (including radiation and large-scale advection) was imposed.

The simulation was performed using the MISU-MIT Cloud and Aerosol model (MIMICA; Savre et al., 2014) as described in Savre and Craig (2023). The numerical domain extends over 102.4 km in both horizontal directions, and the upper boundary is situated 14,250 m above the surface. The horizontal grid spacing is equal to 100 m in both directions, while the vertical grid spacing is constant and equal to 25 m below 1,500 m, but increases geometrically above to reach ∼400 m in the topmost grid layer. Lateral boundaries are periodic, whereas the surface is considered as a free-slip boundary (no momentum fluxes).

The simulation was continued over a period of 10 hr, during which time-dependent variables were extracted every minute. The first clouds are observed 1 hr after the start of the simulation, whereas the onset of surface precipitation occurs 1.5 hr later. Overall, the transition from shallow-to-deep convection happens progressively over the first 7 hr of simulation. In Figure 7a, the mean cloud base and mean cloud top altitudes are shown. Here, the mean cloud base is defined as the level at which the cloud cover is maximum, and the mean cloud top is defined as the first vertical layer from the top where the condensed water mixing ratio exceeds 10^{-3} g kg^{-1}. Clouds are identified at locations where the condensed water mixing ratio exceeds a threshold of 10^{-3} g kg^{-1}. In addition, the LFC is also represented. As one may see, after around 3 hr the mean cloud base altitude is almost identical to the

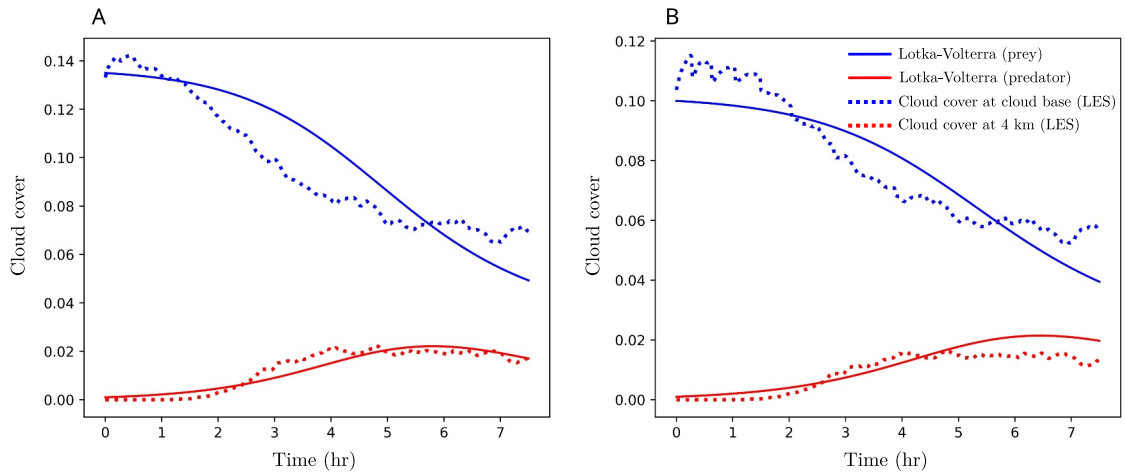

Figure 8. Lotka–Volterra model (solid lines) versus LES data (dotted lines) for the LBA transition case. (a) Cloud cover at the cloud base as prey (blue lines) and cloud cover at 4 km height as predators (red lines). (b) As in (a) but for cloudy updraft cover. For the Lotka–Voltera model, the following coefficients are considered: $a = 0$, $b = 3 \cdot 10^{-3}$ s^{-1}, $e = 3.5 \cdot 10^{-3}$ s^{-1}, $f = 2.5 \cdot 10^{-4}$ s^{-1} (a); and $a = 0$, $b = 3 \cdot 10^{-3}$ s^{-1}, $e = 4 \cdot 10^{-3}$ s^{-1}, $f = 2 \cdot 10^{-4}$ s^{-1} (b). The initial conditions are set to 0.135 for the cloud cover at the cloud base, 0.1 for the cloudy updraft cover at the cloud base, and 10^{-3} for the cloud cover and for the cloudy updraft at 4 km. Here, the initial time is set to 2.5 hr after the start of the simulation.

LFC. The time evolution of CAPE and CIN is also represented in Figure 7b. CIN becomes very small after 2 hr, gradually increasing during the shallow–to–deep transition to about 10 J kg^{-1}. Here, we consider the shallow–to–deep convection transition to begin 2.5 hr after the start of the simulation. During the transition, CAPE increases from about 1600 J kg^{-1} to about 2000 J kg^{-1}. In Figure 7c, the mass flux at the cloud based during the simulation is also shown. Here, the mass flux is computed considering only the grid cells in which the vertical velocity is above a threshold of 0.1 m s^{-1}. As one may see, during the transition, the mass flux also decreases, as also shown by Kurowski et al. (2018), and thus, the first term in Equation 5 might also contribute to the decrease in the total cloud fraction, as explained in Section 2. In addition, the time series of the cloud water path (CWP) is shown in Figure 7d.

The total cloud cover σ and cloud cover associated with precipitating convection σ_c that will be used to validate the predator–prey model are defined as follows. The total cloud cover is computed as the ratio between the number of grid cells identified as cloudy at the mean cloud base altitude to the total number of grid cells at that level. The cloud cover of convective precipitating clouds is defined following the same procedure but 4 km above the surface. In Figure 8a, simulated total and precipitating cloud covers are shown together with a solution of the Lotka–Volterra model in which the cloud fraction at cloud base (total cloud population) is assumed to act as prey, and the cloud fraction at 4 km (precipitating cloud population) is assumed to act as predator. The Lotka–Volterra model is solved using the simple Euler method with 10^4 iterations (a convergence test with 10^3 iterations has been performed, showing no significant difference). Here, the Lotka–Volterra model is represented only to show the predator–prey characteristic of the system, and thus, no objective tuning of coefficients against the LES data has been performed: the coefficients were simply chosen to visually match the LES data. Note that in this paper, we do not try to find the optimal values for the model coefficients, since it is a difficult task (Lunderman et al., 2020) and would require using many different LES simulations for various meteorological situations: it is out of scope for this paper, which just tries to show that the predator-prey model is a valid model to consider. As can be seen from Figure 8a, even a very simple predator–prey system can model reasonably well the rapid transition from shallow to deep continental convection, however, far from being a perfect model. As speculated above, σ_c can indeed act as a predator. We show in particular that the cloud cover decreases as the fraction of convective clouds at a higher level increases. Later, as the total cloud cover decreases, the number of clouds that provide local preconditioning for the subsequent convection also decreases, and thus, the population of predators (precipitating clouds) will decrease as they no longer have enough prey to feed on.

Because the cloudy updrafts are regarded as the fundamental agents of vertical convective transport in the mass–flux parameterization, we also analyze here the predator–prey characteristics of cloud cover with clouds identified

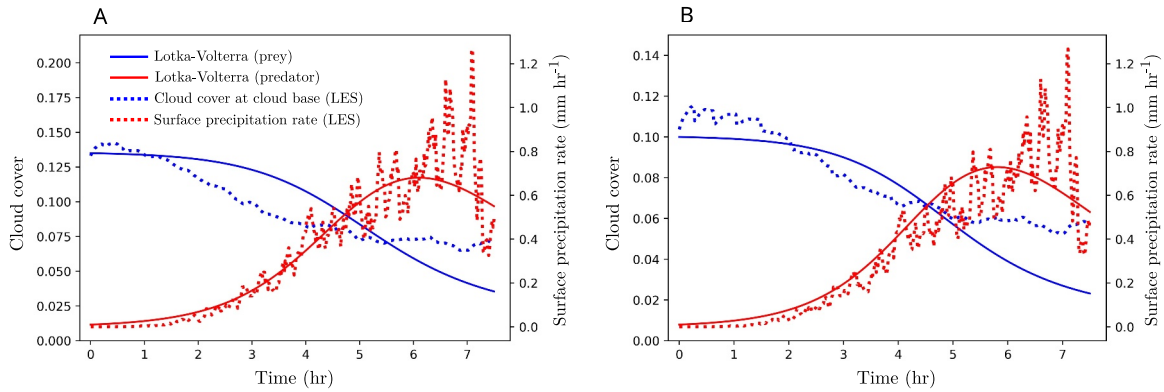

Figure 9. As in Figure 8 but the with surface precipitation rate acting as predators. For the Lotka–Voltera model, the following coefficients are considered: $a = 0$, $b = 1.5 \cdot 10^{-4}$ hr mm^{-1} s^{-1}, $e = 3.5 \cdot 10^{-3}$ s^{-1}, $f = 2 \cdot 10^{-4}$ s^{-1} (a); and $a = 0, b = 1.5 \cdot 10^{-4}$ hr mm^{-1} s^{-1}, $e = 5 \cdot 10^{-3}$ s^{-1}, $f = 2.1 \cdot 10^{-4}$ s^{-1} (b). The initial surface precipitation rate is set to 10^{-3} mm hr^{-1}.

based on an additional updraft criterion. Here, a threshold of 0.1 m s^{-1} is used to identify the cloudy updrafts. The predator–prey characteristics of cloud cover based on this additional updraft criterion (cloudy updraft cover) are presented in Figure 8b. As speculated above, the cloudy updraft cover also follows predator–prey characteristics, like the total cloud population, as indeed the updraft cover and the cloud cover are proportional. The predator–prey characteristics can be seen from the fact that the cloudy updraft cover at cloud base decreases as the cloudy updraft cover at 4 km increases in the first part of the transition. This is followed by a decrease in the cloudy updraft cover at 4 km as the number of prey becomes too small. Note that Yano and Plant (2012b) argue that during the shallow–to–deep transition, as CAPE increases, the cloudy updraft cover at cloud base also increases, but without giving any physical argument to support this assertion. However, it is quite clear from Figure 8b that for the rapid shallow–to–deep transition discussed here, the cloud cover at the cloud base exhibits a decrease during the transition, even though CAPE does increase.

As a first order approximation, we can consider that the surface precipitation rate P is directly proportional to σ_c. Similar to Koren and Feingold (2011), we may therefore replace σ_c with P in Equations 7 and 8, thus considering that the surface precipitation rate acts as a predator that preys on the total cloud fraction. We then expect to see a time series for the cloud–precipitation system resembling that displayed in Figure 5a, and a solution for the cloud cover and precipitation rate similar to the one shown in Figure 5b.

In Figure 9, the time series of cloud cover at cloud base and surface precipitation rate are presented, together with a solution of the Lotka–Volterra model in which the cloud fraction at cloud base is assumed to act as prey, and the surface precipitation rate is assumed to act as predator. The surface precipitation rate displayed in Figure 9 represents the domain–averaged surface precipitation rate. Indeed, the cloud–precipitations system exhibits predator–prey characteristics during the rapid shallow–to–deep transition, as speculated above. Although not perfect, the Lotka–Volterra model does seem to represent reasonably well the interaction between clouds and precipitation.

3.2. Extension to a Three Species Model

An extension to a three species model can be made by considering that the convective precipitating clouds can be further classified as congestus and cumulonimbus clouds. Here, we consider that the congestus clouds are those clouds with a top between 4 and 8 km, whereas the cumulonimbus clouds have a top above 8 km. Therefore, we consider that the cloud cover at the cloud base (total cloud population) acts as prey for the cloud cover at 4 km σ_c (convective precipitating cloud population), which also represents the prey for the cloud cover at 8 km σ_{cb} (cumulonimbus cloud cover). Hence, we have the following predator–prey system:

$$\frac{d\sigma}{dt} = \beta_1 \sigma - \beta_2 \sigma \sigma_c, \tag{16}$$

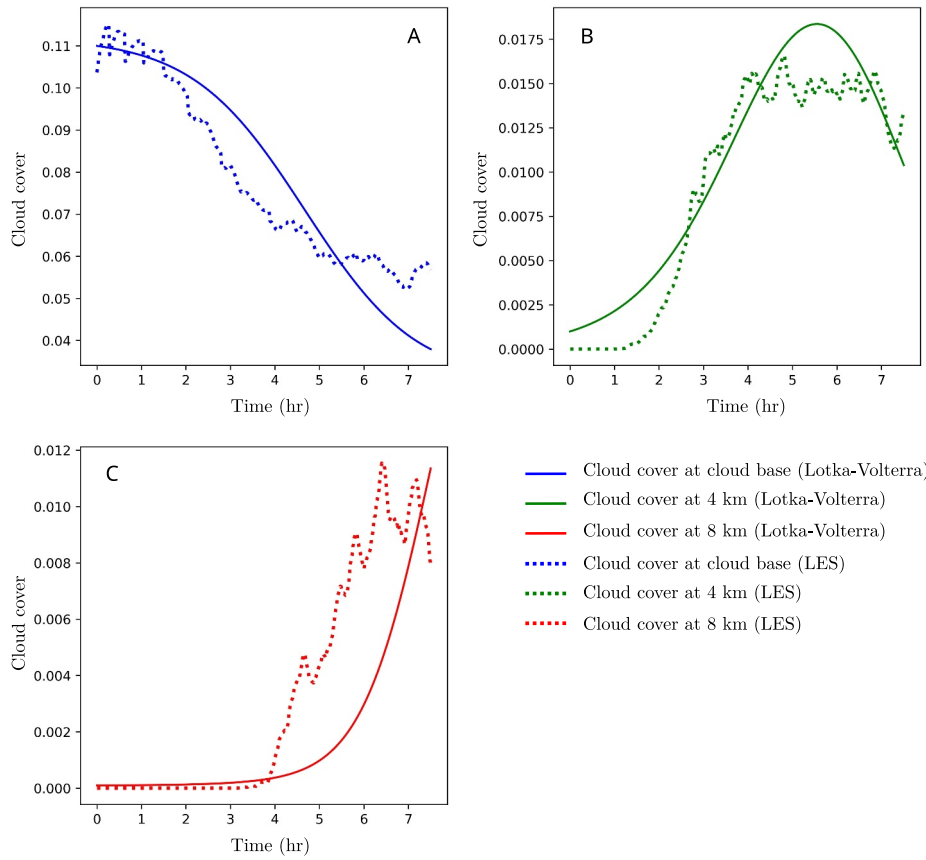

Figure 10. Three species Lotka–Volterra model (solid lines) versus LES data (dotted lines) for the LBA transition case. (a) Cloudy updraft cover at the cloud base as prey (blue lines); (b) Cloudy cover at the 4 km height representing the convective fractional area of congestus and cumulonimbus clouds; (c) Cloudy cover at the 8 km height representing the convective fractional area of cumulonimbus clouds. For the Lotka–Voltera model, the following coefficients are considered: $\beta_1 = 0, \beta_2 = 3.8 \cdot 10^{-3}\ \mathrm{s}^{-1}, \beta_3 = 3.8 \cdot 10^{-3}\ \mathrm{s}^{-1}, \beta_4 = 10^{-2}\ \mathrm{s}^{-1}, \beta_5 = 2 \cdot 10^{-4}\ \mathrm{s}^{-1}, \beta_6 = 1.7 \cdot 10^{-2}\ \mathrm{s}^{-1}, \beta_7 = 10^{-6}\ \mathrm{s}^{-1}$. The initial conditions are set to 0.11, 10^{-3}, and 10^{-4} for the cloudy updraft cover at the cloud base, at 4 km, and 8 km, respectively.

$$\frac{d\sigma_c}{dt} = \beta_3 \sigma \sigma_c - \beta_4 \sigma_c \sigma_{cb} - \beta_5 \sigma_c, \tag{17}$$

$$\frac{d\sigma_{cb}}{dt} = \beta_6 \sigma_c \sigma_{cb} - \beta_7 \sigma_{cb}, \tag{18}$$

where β_1–β_7 are system coefficients. A solution to this system is presented in Figure 10, together with time series of cloud cover at the cloud base (Figure 10a), 4 km (Figure 10b), and 8 km (Figure 10c), from the LBA transition case described above. Comparing the LES data for the cloud cover at these three levels with the solution of the Lotka–Volterra model, the system seems to exhibit predator–prey characteristics with three species.

A further extension to n_z species, where n_z represents the number of vertical levels used by the parent numerical model, follows immediately. For the updraft fractional area σ_k at the vertical level k, we now have:

$$\frac{d\sigma_k}{dt} = a_{k,k-1} \sigma_k \sigma_{k-1} - a_{k,k+1} \sigma_k \sigma_{k+1} + r_k \sigma_k, \tag{19}$$

where $a_{k,k-1}$, $a_{k,k+1}$, and r_k are system coefficients. The number of species represents the number of vertical levels of the parent numerical model between LFC and the equilibrium level.

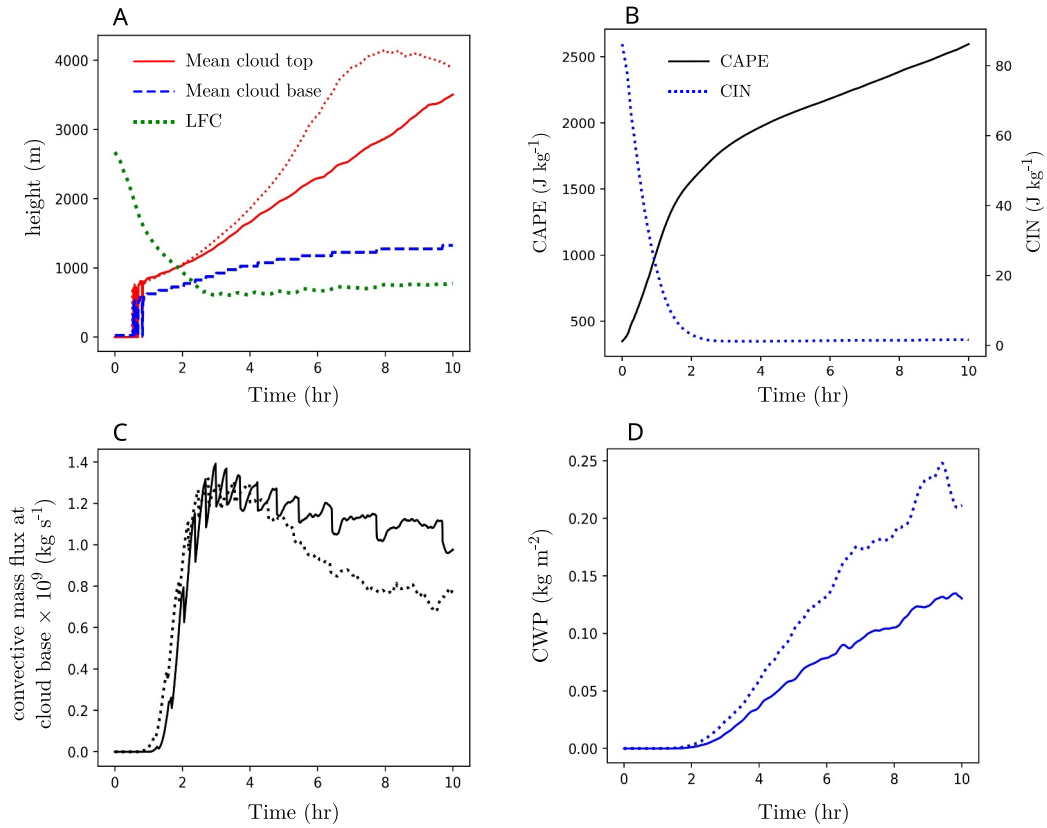

Figure 11. As in Figure 7, but for the case with suppressed cold pools. The mean cloud top for the case with active cold pools is also displayed in (a) with red dotted line. Similarly, the convective mass flux at cloud base and cloud water path for the case with active cold pools are also plotted in (c) and (d), respectively, with dotted lines.

3.3. LBA Transition Case With Suppressed Cold Pools

As discussed in Section 2, in our conceptual model, the predator–prey characteristics for the shallow–to–deep transition is due to the local moisture preconditioning, with the cold pool feedback only acting as a reinforcement. Thus, we argue that predator–prey behavior is expected even in the absence of the cold pools. To test this aspect, an additional simulation with suppressed cold pools is performed. The strategy proposed by Böing et al. (2012) was adopted here whereby potential temperature and water vapor mixing ratio tendencies below cloud base are nudged to their horizontally averaged values with a time scale of 10 min.

In Figure 11a, the mean cloud top, mean cloud base, and LFC are presented. The mean cloud top for the case with active cold pools is also presented here to better appreciate the cold pool feedback in the shallow–to–deep transition. As expected, the transition is slower for the case with suppressed cold pools, although there is not a large difference between the mean cloud top for the two cases in the first part of the transition, during which we argue that the role of local preconditioning is the main mechanism responsible for the transition. As another interesting aspect, in this case, the LFC is lower than the mean cloud base during the shallow–to–deep transition. As in the case with active cold pools, we consider that the transition starts at 2.5 hr after the start of the simulation, but the cloud top does not reach a maximum even after 10 hr, at the end of the simulation. The time series for CAPE and CIN is represented in Figure 11b. Although CAPE increases in a similar fashion to the case with active cold pools, CIN reaches a minimum after around 2.5 hr, remaining rather constant during the transition, at a value of about 1.5 J kg^{-1}. In addition, LFC is also much lower in the case with suppressed cold pools (around 0.7 km) than in the case with active cold pools (around 1 km). The convective mass flux at cloud base and the CWP are also shown in Figures 11c and 11d, respectively. As one may see, the cold pools contribute to the reduction of the mass flux at the cloud base during the transition, but also to a more rapid deepening of the cumulus clouds.

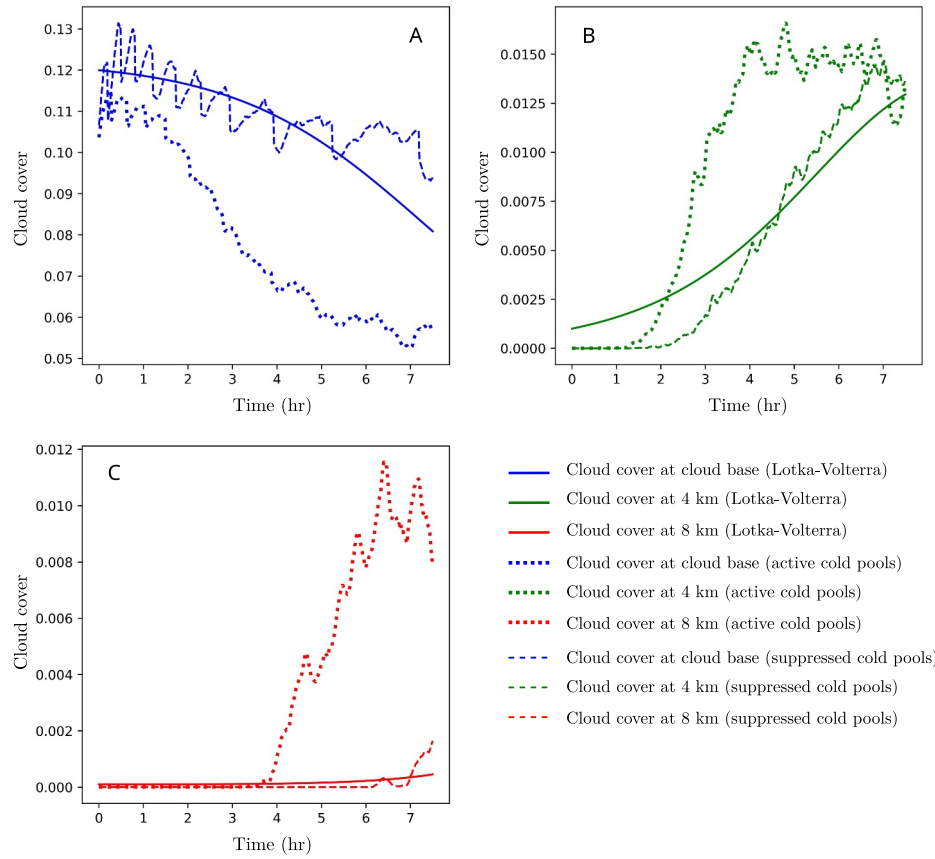

Figure 12. As in Figure 10, but for the case with suppressed cold pools. The cloudy updraft covers for the case with active cold pools are also displayed here with dotted lines, while the cloudy updraft covers for the case with suppressed cold pools are represented with dashed lines. For the Lotka–Voltera model, the following coefficients are considered: $\beta_1 = 0$, $\beta_2 = 2.5 \cdot 10^{-3}\ s^{-1}, \beta_3 = 2.5 \cdot 10^{-3}\ s^{-1}, \beta_4 = 10^{-2}\ s^{-1}, \beta_5 = 1.7 \cdot 10^{-4}\ s^{-1}, \beta_6 = 1.3 \cdot 10^{-2}\ s^{-1}, \beta_7 = 2 \cdot 10^{-5}\ s^{-1}$. The initial conditions are set to 0.12, 10^{-3}, and 10^{-4} for the cloudy updraft cover at the cloud base, at 4 km, and 8 km, respectively.

In Figure 12, the cloudy updraft covers at cloud base, 4 km, and 8 km, are represented for the case with suppressed cold pools, together with a solution of the three species Lotka–Voltera model. As speculated, even without cold pools, the system seems to exhibit predator–prey characteristics. In order to appreciate the role of the cold pool feedback in the transition, we also represent the cloudy updrafts covers for the case with active cold pools. As we expected from the conceptual model, without cold pool feedback the predators are not that efficient in preying on the total cloud population, and thus the cloud cover at the cloud base does not decrease as fast as the cloud cover for the case with active cold pools, while the populations of convective precipitating clouds and cumulonimbus clouds are not able to grow as fast and as much as for the case with active cold pools. Moreover, with suppressed cold pools, a larger number of updrafts are able to reach the condensation level as CIN is lower and there is no organization of the updraft field in the boundary layer.

Although there is a significant difference in the number of cumulonimbus clouds between the two simulations, it is clear that the deepening of cumulus convection is possible even without cold pools feedback. This aspect, together with the predator–prey characteristics of the case with suppressed cold pools, indicates that the local preconditioning plays a major role in the shallow–to–deep transition, as also argued by Vraciu et al. (2023), and we believe that much more attention should be given to the local moisture preconditioning, and to the interplay between the local preconditioning and cold pools feedback during the transition from shallow to precipitating convection. We schematically present the feedback loops between the clouds and cold pools in our conceptual model on Figure 13. A negative feedback loop between the total cloud cover and precipitating cloud cover is possible without the presence of the cold pools, due to local preconditioning and mass continuity, implying a

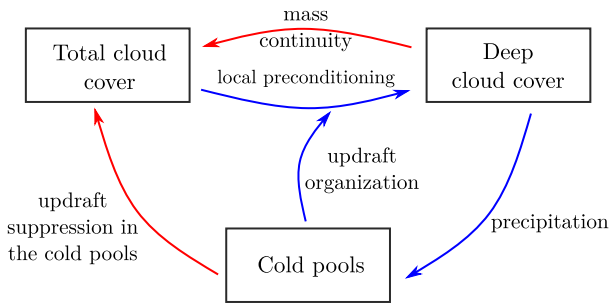

Figure 13. Schematics of feedback between the clouds and cold pools. The blue arrow denotes a positive causality, while the red one denotes a negative causality.

predator–prey–type of interaction between the two. As the precipitating clouds start to precipitate in their decaying state, cold pools are formed in the boundary layer, which have a positive effect on the population of precipitating clouds, but also a direct negative effect on the total cloud cover due to the suppression of updrafts in the cold pools, as discussed in Section 2.2. As the cold pools have a positive feedback on the population of precipitating clouds, due to mass continuity, the cold pools also have an indirect negative effect on the total cloud cover, as also schematically illustrated in Figure 4. Here, the blue arrow from the cold pools points toward local preconditioning, as in our conceptual model the cold pools, through the organization of updrafts, increase the probability of updrafts feeding into preexisting clouds, and thus, leading to a larger degree of local preconditioning, as also discussed in Section 2.2. Therefore, the interaction coefficients β_2, β_3, β_4, and β_6 are larger for the case with active cold pools. Overall, the cold pools amplify the feedback loop between the total cloud cover (prey) and the precipitating cloud cover (predator), which can be seen as making the predators more efficient in catching the prey. In this sense perhaps, the cold pools may be seen as mountains forcing the prey and predators to live into narrow valleys (the gust fronts), thus facilitating the interactions between them. The decay coefficient β_5, associated with the decaying rate of congestus clouds, is also larger in the presence of the cold pools. Without further analyses, we can only speculate that this is due to the fact that the stronger cumulonimbus clouds forming in the presence of cold pools lead to larger subsidence of dry air into the lower parts of the troposphere, thus making congestus clouds more susceptible to evaporation through lateral entrainment (Equation 12). On the other hand, the decay coefficient β_7, associated with the decaying rate of cumulonimbus clouds, is smaller for the case with active cloud pools, which might indicate the fact that because the cumulonimbus clouds are wider in the presence of the cold pools (Schlemmer & Hohenegger, 2014), they are less susceptible to mixing with the environment.

3.4. Complete Diurnal Cycle

To see if within a complete diurnal cycle the cloud–precipitation system exhibits predator–prey characteristics, we consider here the idealized case reported in Jensen et al. (2022) that is openly available at Haerter (2021). The reader is referred to Jensen et al. (2022) for case description and methodological details. In a complete diurnal cycle, we can no longer ignore the contribution of the surface heat flux on σ. Thus, we can no longer assume that the Lotka–Volterra system, in which the coefficients a, b, e, and f are assumed constant, can describe the interaction between the cloud cover and precipitation rate. However, during the transition from shallow to precipitation convection, we still expect to see a predator–prey type of interaction.

In Figure 14, the LES data for cloud cover and surface precipitation from Jensen et al. (2022) are represented. In the morning, during the onset of the shallow convection, the cloud population increases as more and more updrafts are able to overcome the transition layer and reach the condensation level, and thus, the evolution of the cloud fraction is dominated by the diurnal forcing associated with the surface fluxes. As CIN approaches zero, the transition from shallow to precipitation convection starts, and indeed, during this short period, we see predator–prey characteristics in the cloud–precipitation system (Figure 14a), which correspond to the upper–right portion of the limit–cycle (Figure 14b). Thus, during the transition, in agreement with our conceptual model, the cloud fraction decreases as the precipitation rate increases, which in turn leads to a reduction in the precipitation rate. During the evening, the surface heat flux is unable to provide enough energy into the system, and CIN is slowly restored. Thus, the cloud fraction decreases as the clouds that decay are no longer replaced by new active clouds, and the cloud population is again controlled by the diurnal forcing.

Although Figure 14 suggests that even within a complete diurnal cycle the system exhibits predator–prey characteristics, our simple Lotka–Volterra model is only able to represent the transition phase happening during the day. The model is indeed unable to represent the simultaneous decay of both shallow and deep cumuli at night when the reduced surface fluxes cannot sustain convection. A predator–prey model that takes into consideration this diurnal forcing might however be designed and adjusted to reproduce the complete diurnal cycle of cloud and precipitation. A possible path toward such a system might be the use of the predator–prey system derived in Section 2.3 but with additional dynamical equations for w_0, $CAPE$ and R_E in which a, b, e, and f are no longer constants. Such a development will be considered in future work.

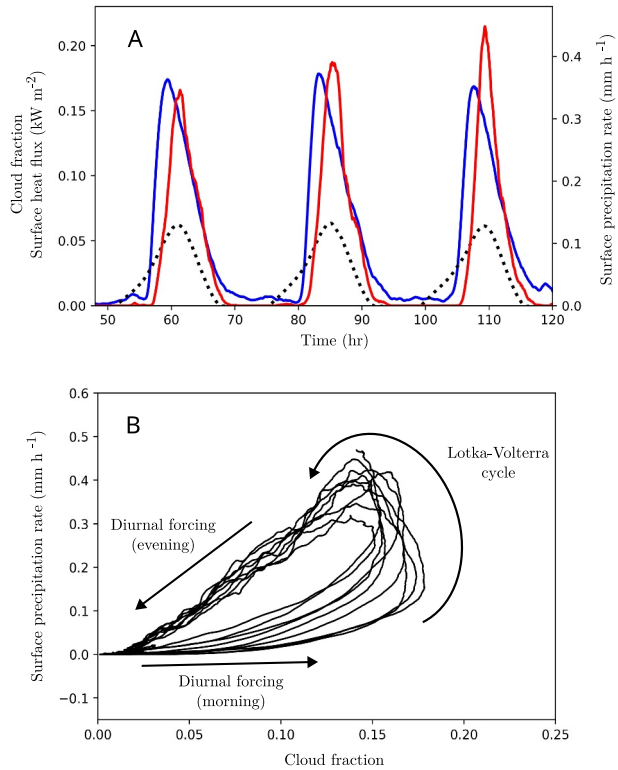

Figure 14. Large-eddy simulation of the cloud–precipitation system in a complete diurnal cycle from Jensen et al. (2022). (a) Time series for cloud fraction (blue solid line) and surface precipitation rate (red solid line) for three complete diurnal cycles. The surface heat flux is also represented for reference (dotted black line). (b) Limit–cycle of the cloud–precipitation system for the complete simulation (10 days), except the first 2 days, which are considered spin–up time.

4. Discussion and Conclusions

In this study, we consider that the cumulus clouds are formed due to the upward transport of water vapor from the boundary layer by multiple convective elements, as suggested by empirical evidence. As the clouds themselves precondition their local surroundings for the subsequent convective updrafts, it is considered that the convective precipitating clouds act as predators, eating from the total cloud fraction that sustains their growth. As the clouds become deeper, the total cloud fraction decreases, and thus, the total cloud population can be seen as the prey population in a predator–prey system. It is also argued that the cold pool feedback acts as a reinforcement mechanism, leading to more clustered convection. The conceptual picture for the shallow-to-deep convection reminds us of the transition from unorganized to aggregated convection, but at a smaller scale. Therefore, we argue that the very complex cloud dynamics in the rapid shallow–to–deep transition of atmospheric convection can be described by the very simple Lotka–Volterra predator–prey system if it is assumed that the change in the large–scale state is slow enough during the transition. We tested a simple predator–prey model against idealized high–resolution LES data, showing good agreement between them. To isolate the role of local moisture preconditioning from that of cold pool feedback, we also consider a twin LES simulation with suppressed cold pools. In agreement with our conceptual model, the transition displays predator–prey characteristics even without cold pools, which might be an indication that the local preconditioning plays an important role in the shallow–to–deep transition. Finally, we discuss the complete diurnal cycle of deep convection, showing that the cloud population also exhibits a predator–prey–type of behavior in this situation. We consider that future research is required to study in depth every causality implied by our study, which might help us better understand the complex process of storm formation and convective organization.

In a diurnal cycle of deep continental convection, the predator–prey model assumes a gradual transition to deep convection instead of assuming an instantaneous deep convection triggering. The majority of current mass–flux schemes for deep convection consider a constant fractional area occupied by the convection, either explicitly or implicitly. However, in a rapid transition from shallow to precipitating deep convection, the environmental state only exhibits a small change, and the convective mass–flux is primarily controlled by convective fractional area and not by the vertical velocity. Therefore, our predator–prey model may be implemented for such a case by replacing the mass–flux predicted by the deep convection scheme M_c' with an adjusted mass–flux $M_{c,adj}$, as follows:

$$M_{c,adj} = \frac{\sigma_c}{\sigma_c'} M_c', \tag{20}$$

where σ_c is the fraction of convective precipitating clouds from the predator–prey model, and σ_c' is the constant fractional area assumed by the deep convection schemes. If the scheme does not assume a fractional area in an explicit way, then a constant value for σ_c' must be prescribed. Therefore, a predator–prey model may be implemented in a weather prediction or climate numerical model, obtaining a cumulus parameterization scheme with convective memory, that is based on a more realistic conceptual picture than the traditional mass–flux formulation, that goes beyond the one-cloud equals one-updraft framework. It should be noted, however, that this implementation cannot be made if the deep convective scheme already has a parameterization for the cold pool feedback (e.g., Rio et al., 2009; Suselj et al., 2019), as this would lead to a "double counting" of the cold pools effect. Such an implementation, however, can only be made during the shallow–to–deep transition, as it is considered that the environment does not change substantially. Therefore, the predator–prey model must only be turned on when the conditions for deep convection onset are met and turned off after deep convection fully develops. Moreover, as shown in Section 3.2, the predator–prey system can be further generalized, to predict the convective fractional area at every vertical level of the numerical model. Future research is required to find the most appropriate predator–prey system for the shallow–to–deep transition and to tune the various coefficients introduced by the model.

As another very important contribution of the present conceptual model, a unified convection–cloud picture is described in which both clouds and convective elements interact with each other. Thus, the present predator–prey model also provides a parameterization for the total cumulus fraction, a problem notorious for the climate projections (e.g., Vogel et al., 2022). In addition, a complete unified parameterization might be built based on the principles introduced here by considering the prognostic system of Equations 10 and 14 for the cloud fractions, and a bulk plume model that considers the local preconditioning to model the updraft velocity w_c, as proposed for example, by Vraciu et al. (2023). Furthermore, note that by considering the system of Equations 10 and 14, the boundary layer control of deep convection is implicit, in contrast with the traditional mass–flux formulation in which a boundary layer control, although considered by many modern parameterizations, might be in fact inconsistent with the steady–state plume model of the mass–flux formulation (please refer to Yano et al. (2013) for a detailed discussion of this issue). Such a development is not presented here but left for future work.

Appendix A: Proportionality Between Cloud Cover and Updraft Cover

An important step in the derivation of the Lotka–Volterra model in Section 2.3 is the assumption that the updraft cover and the cloud cover are proportional, considered in Equation 11 at both cloud base and at 4 km altitude. In Figure A1, the cloud cover and the cloudy updraft cover are represented for the two LBA transition cases analyzed in Section 3. The figure shows that indeed the updraft cover is proportional to the cloud cover at both cloud base and at 4 km altitude, with a proportionality coefficient of about 0.8.

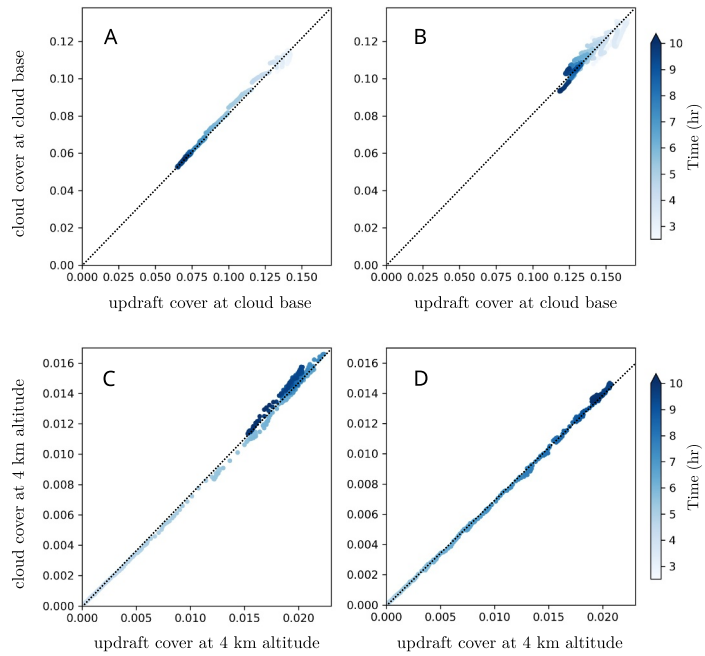

Figure A1. Cloudy updraft cover versus cloud cover at cloud base (a), (b) and at 4 km altitude (c), (d) for the LBA transition case with active cold pools (a), (c) and for the LBA transition case with suppressed cold pools (b), (d).

Appendix B: The Parameterization of Function $F(R_{E1},\sigma)$

In Section 2.3 we consider that the updraft velocity at the base of the second layer is given by Equation 15, where $F(R_{E1},\sigma)$ is a function assumed to represent the local preconditioning in our conceptual model. In the first layer we consider two types of updrafts: (a) interacting updrafts: updrafts developing within preexisting clouds, as discussed in Section 2, and (b) non-interacting updrafts, developing in the dry environment. Thus, the vertical velocity w_c can be written as a mean over the two types of updrafts, as follows:

$$w_c = \frac{w_{c,ni}\sigma_{c,ni} + w_{c,i}\sigma_{c,i}}{\sigma_0}, \tag{B1}$$

where $w_{c,ni}$ and $\sigma_{c,ni}$ are the vertical velocity and fractional area of the non-interacting convective updrafts, respectively, $w_{c,i}$ and $\sigma_{c,i}$ are the vertical velocity and fractional area of the interacting convective updrafts, respectively, and σ_0 is the updraft fractional area in the first cloud layer. Here, the updrafts velocities are evaluated at the top of the first cloud layer (base of the second cloud layer), and the updraft fractional area are assumed constant through the first cloud layer, and thus, they can be evaluated at the base of the first layer. As argued in Section 2, we consider that the precipitating cumulus clouds are formed by the contribution of multiple convective elements contributing to their development, and thus, we argue that the updrafts at the base of the second cloud layer are mostly interacting, implying that $w_{c,ni}\sigma_{c,ni} \ll w_{c,i}\sigma_{c,i}$, which gives $w_c \approx w_{c,i}\sigma_{c,i}/\sigma_0$. We further assume that the fraction of interacting updrafts is proportional to the cloud cover at the cloud base as:

$$\sigma_{c,i} = p_{int}\sigma_0\sigma, \tag{B2}$$

where p_{int} represents a parameter associated with the interaction probability between the updrafts and the pre-existing clouds. If the updrafts develop in completely random placed at LCL, then $p_{int} = 1$, but if the preexisting clouds make it easier for the updrafts to reach LCL in their places, as argued in Section 2.1, then the updrafts will "prefer" to develop within the preexisting clouds, implying that $p_{int} > 1$. Considering that $w_{c,i}$ is proportional to $\sqrt{2CAPE}$, we obtain:

$$w_c = p_{int}\sigma a_0\sqrt{2CAPE}, \tag{B3}$$

where a_0 is a parameter associated with the entrainment and pressure gradients upon the convective elements. The interacting updrafts interact with passive cloud volumes (PCVs) (Vraciu et al., 2023). The PCVs are subject to evaporation into the environment at a rate that strongly depends on the environmental relative humidity. Therefore, the lifetime of the PCVs in the first cloud layer depends on $\mathcal{R}_{E1}$. Thus, the parameter p_{int} must also depend on the lifetime of the PCVs τ_{PCV} and the time between two consecutive updrafts τ_{up}. If $\tau_{PCV} < \tau_{up}$, then the PCVs are already dissipated at the time a subsequent updraft reaches LCL, and thus, $p_{int} = 0$. On the other hand, if $\tau_{PCV} \gg \tau_{up}$, we expect $p_{int} \to 1/\sigma$, as any updraft will develop within a PCV created by the previous updraft. Note that $\tau_{PCV} \gg \tau_{up}$ corresponds to a case in which $\mathcal{R}_{E1} = 100\%$ and $\sigma \to 1$. Therefore, we consider that p_{int} is a function of the environmental relative humidity as:

$$p_{int} = c\mathcal{R}_{E1}^{\epsilon}, \tag{B4}$$

where c is a parameter associated with convective organization and ϵ is a positive exponent. Combining thus Equations B3 and B4, we obtain:

$$w_c = a_0 c\sqrt{2CAPE}\ \mathcal{R}_{E1}^{\epsilon}\sigma. \tag{B5}$$

Data Availability Statement

The LES data presented in Sections 3.1 and 3.2 of this work are openly available at Savre (2023a), while the data presented in Section 3.3 are available at Savre (2023b). The data presented in Figure 14 are openly available at Haerter (2021).

Acknowledgments
We thank Robert Plant for discussions on an earlier version of the manuscript. We also acknowledge the insightful comments and suggestions from the anonymous reviewers, which greatly improved the quality of our work. CVV acknowledges financial support from the Romanian Ministry of Research, Innovation, and Digitization through Project PN 23 21 01 01.

References

Albright, A. L., Bony, S., Stevens, B., & Vogel, R. (2022). Observed subcloud-layer moisture and heat budgets in the trades. *Journal of the Atmospheric Sciences*, *79*(9), 2363–2385. https://doi.org/10.1175/jas-d-21-0337.1

Albright, A. L., Stevens, B., Bony, S., & Vogel, R. (2023). A new conceptual picture of the trade wind transition layer. *Journal of the Atmospheric Sciences*, *80*(6), 1547–1563. https://doi.org/10.1175/jas-d-22-0184.1

Arakawa, A. (2004). The cumulus parameterization problem: Past, present, and future. *Journal of Climate*, *17*(13), 2493–2525. https://doi.org/10.1175/1520-0442(2004)017<2493:ratcpp>2.0.co;2

Arakawa, A., & Schubert, W. H. (1974). Interaction of a cumulus cloud ensemble with the large-scale environment, Part I. *Journal of the Atmospheric Sciences*, *31*(3), 674–701. https://doi.org/10.1175/1520-0469(1974)031<0674:ioacce>2.0.co;2

Bechtold, P., Bazile, E., Guichard, F., Mascart, P., & Richard, E. (2001). A mass-flux convection scheme for regional and global models. *Quarterly Journal of the Royal Meteorological Society*, *127*(573), 869–886. https://doi.org/10.1002/qj.49712757309

Bechtold, P., Chaboureau, J.-P., Beljaars, A., Betts, A., Köhler, M., Miller, M., & Redelsperger, J.-L. (2004). The simulation of the diurnal cycle of convective precipitation over land in a global model. *Quarterly Journal of the Royal Meteorological Society*, *130*(604), 3119–3137. https://doi.org/10.1256/qj.03.103

Bechtold, P., Semane, N., Lopez, P., Chaboureau, J.-P., Beljaars, A., & Bormann, N. (2014). Representing equilibrium and nonequilibrium convection in large-scale models. *Journal of the Atmospheric Sciences*, *71*(2), 734–753. https://doi.org/10.1175/jas-d-13-0163.1

Betts, A. K. (1976). Modeling subcloud layer structure and interaction with a shallow cumulus layer. *Journal of the Atmospheric Sciences*, *33*(12), 2363–2382. https://doi.org/10.1175/1520-0469(1976)033<2363:mslsai>2.0.co;2

Böing, S. J., Jonker, H. J. J., Siebesma, A. P., & Grabowski, W. W. (2012). Influence of the subcloud layer on the development of a deep convective ensemble. *Journal of the Atmospheric Sciences*, *69*(9), 2682–2698. https://doi.org/10.1175/JAS-D-11-0317.1

Bretherton, C. S., McCaa, J. R., & Grenier, H. (2004). A new parameterization for shallow cumulus convection and its application to marine subtropical cloud-topped boundary layers. Part I: Description and 1D results. *Monthly Weather Review*, *132*(4), 864–882. https://doi.org/10.1175/1520-0493(2004)132<0864:anpfsc>2.0.co;2

Champouillon, A., Rio, C., & Couvreux, F. (2023). Simulating the transition from shallow to deep convection across scales: The role of congestus clouds. *Journal of the Atmospheric Sciences*, *80*(12), 2989–3005. https://doi.org/10.1175/jas-d-23-0027.1

Christopoulos, C., & Schneider, T. (2021). Assessing biases and climate implications of the diurnal precipitation cycle in climate models. *Geophysical Research Letters*, *48*(13), e2021GL093017. https://doi.org/10.1029/2021gl093017

Colin, M., Sherwood, S., Geoffroy, O., Bony, S., & Fuchs, D. (2019). Identifying the sources of convective memory in cloud-resolving simulations. *Journal of the Atmospheric Sciences*, *76*(3), 947–962. https://doi.org/10.1175/jas-d-18-0036.1

Colin, M., & Sherwood, S. C. (2021). Atmospheric convection as an unstable predator–prey process with memory. *Journal of the Atmospheric Sciences*, *78*(11), 3781–3797. https://doi.org/10.1175/jas-d-20-0337.1

Couvreux, F., Roehrig, R., Rio, C., Lefebvre, M.-P., Komori, T., Derbyshire, S., et al. (2015). Representation of daytime moist convection over the semi-arid tropics by parametrizations used in climate and meteorological models. *Quarterly Journal of the Royal Meteorological Society*, *141*(691), 2220–2236. https://doi.org/10.1002/qj.2517

Daleu, C. L., Plant, R., Woolnough, S., Stirling, A., & Harvey, N. (2020). Memory properties in cloud-resolving simulations of the diurnal cycle of deep convection. *Journal of Advances in Modeling Earth Systems*, *12*(8), e2019MS001897. https://doi.org/10.1029/2019ms001897

Damiani, R., Vali, G., & Haimov, S. (2006). The structure of thermals in cumulus from airborne dual-Doppler radar observations. *Journal of the Atmospheric Sciences*, *63*(5), 1432–1450. https://doi.org/10.1175/jas3701.1

Davies, L., Plant, R., & Derbyshire, S. (2013). Departures from convective equilibrium with a rapidly varying surface forcing. *Quarterly Journal of the Royal Meteorological Society*, *139*(676), 1731–1746. https://doi.org/10.1002/qj.2065

Donner, L. J. (1993). A cumulus parameterization including mass fluxes, vertical momentum dynamics, and mesoscale effects. *Journal of the Atmospheric Sciences*, *50*(6), 889–906. https://doi.org/10.1175/1520-0469(1993)050<0889:acpimf>2.0.co;2

Donner, L. J., & Phillips, V. T. (2003). Boundary layer control on convective available potential energy: Implications for cumulus parameterization. *Journal of Geophysical Research*, *108*(D22), 4701. https://doi.org/10.1029/2003jd003773

Emanuel, K. A. (1991). A scheme for representing cumulus convection in large-scale models. *Journal of the Atmospheric Sciences*, *48*(21), 2313–2329. https://doi.org/10.1175/1520-0469(1991)048<2313:asfrcc>2.0.co;2

Emanuel, K. A. (1993). A cumulus representation based on the episodic mixing model: The importance of mixing and microphysics in predicting humidity. In *The representation of cumulus convection in numerical models* (pp. 185–192). Springer.

Feingold, G., Koren, I., Yamaguchi, T., & Kazil, J. (2015). On the reversibility of transitions between closed and open cellular convection. *Atmospheric Chemistry and Physics*, *15*(13), 7351–7367. https://doi.org/10.5194/acp-15-7351-2015

Grabowski, W. (2023). Daytime convective development over land: The role of surface forcing. *Quarterly Journal of the Royal Meteorological Society*, *149*(756), 2800–2819. https://doi.org/10.1002/qj.4532

Grabowski, W., Bechtold, P., Cheng, A., Forbes, R., Halliwell, C., Khairoutdinov, M., et al. (2006). Daytime convective development over land: A model intercomparison based on LBA observations. *Quarterly Journal of the Royal Meteorological Society*, *132*(615), 317–344. https://doi.org/10.1256/qj.04.147

Haerter, J. O. (2021). 1D (time) and 2D (time and vertical coordinate) data for the cases DIU-500m, RCE-500m and DIU2RCE-500m [Dataset]. *Zenodo*. https://doi.org/10.5281/zenodo.4898182

Harrington, E. L. (1958). Observations on the appearance and growth of tropical cumuli. *Journal of the Atmospheric Sciences*, *15*(2), 127–130. https://doi.org/10.1175/1520-0469(1958)015<0127:ootaag>2.0.co;2

Harvey, N. J., Daleu, C. L., Stratton, R. A., Plant, R. S., Woolnough, S. J., & Stirling, A. J. (2022). The impact of surface heterogeneity on the diurnal cycle of deep convection. *Quarterly Journal of the Royal Meteorological Society*, *148*(749), 3509–3527. https://doi.org/10.1002/qj.4371

Hernandez-Deckers, D., & Sherwood, S. C. (2016). A numerical investigation of cumulus thermals. *Journal of the Atmospheric Sciences*, *73*(10), 4117–4136. https://doi.org/10.1175/jas-d-15-0385.1

Herzmann, D. (2017). Turkey tower. Retrieved from https://www.youtube.com/watch?v=LqgWYCMYtDU

Heus, T., Jonker, H. J. J., Van den Akker, H. E., Griffith, E. J., Koutek, M., & Post, F. H. (2009). A statistical approach to the life cycle analysis of cumulus clouds selected in a virtual reality environment. *Journal of Geophysical Research*, *114*(D6), D06208. https://doi.org/10.1029/2008jd010917

Hohenegger, C., & Stevens, B. (2013). Preconditioning deep convection with cumulus congestus. *Journal of the Atmospheric Sciences*, *70*(2), 448–464. https://doi.org/10.1175/jas-d-12-089.1

Holloway, C. E., & Neelin, J. D. (2009). Moisture vertical structure, column water vapor, and tropical deep convection. *Journal of the Atmospheric Sciences*, *66*(6), 1665–1683. https://doi.org/10.1175/2008jas2806.1

Hourdin, F., Couvreux, F., & Menut, L. (2002). Parameterization of the dry convective boundary layer based on a mass flux representation of thermals. *Journal of the Atmospheric Sciences*, *59*(6), 1105–1123. https://doi.org/10.1175/1520-0469(2002)059<1105:potdcb>2.0.co;2

Hwong, Y.-L., Colin, M., Aglas-Leitner, P., Muller, C. J., & Sherwood, S. C. (2023). Assessing memory in convection schemes using idealized tests. *Journal of Advances in Modeling Earth Systems*, *15*(12), e2023MS003726. https://doi.org/10.1029/2023ms003726

Jensen, G. G., Fiévet, R., & Haerter, J. O. (2022). The diurnal path to persistent convective self-aggregation. *Journal of Advances in Modeling Earth Systems*, *14*(5), e2021MS002923. https://doi.org/10.1029/2021ms002923

Jones, T. R., & Randall, D. A. (2011). Quantifying the limits of convective parameterizations. *Journal of Geophysical Research*, *116*(D8), D08210. https://doi.org/10.1029/2010jd014913

Kain, J. S., & Fritsch, J. M. (1993). Convective parameterization for mesoscale models: The Kain-Fritsch scheme. In *The representation of cumulus convection in numerical models* (pp. 165–170). Springer.

Khairoutdinov, M., & Randall, D. (2006). High-resolution simulation of shallow-to-deep convection transition over land. *Journal of the Atmospheric Sciences*, *63*(12), 3421–3436. https://doi.org/10.1175/jas3810.1

Kjoenbongarit. (2013). Forming cumulonimbus (timelapse). Retrieved from https://www.youtube.com/watch?v=232LFz-aiz4

Koenig, L. R. (1963). The glaciating behavior of small cumulonimbus clouds. *Journal of the Atmospheric Sciences*, *20*(1), 29–47. https://doi.org/10.1175/1520-0469(1963)020<0029:tgbosc>2.0.co;2

Koren, I., & Feingold, G. (2011). Aerosol–cloud–precipitation system as a predator-prey problem. *Proceedings of the National Academy of Sciences of the United States of America*, *108*(30), 12227–12232. https://doi.org/10.1073/pnas.1101777108

Kurowski, M. J., Paris, A., & Teixeira, J. (2024). The unique behavior of vertical velocity in developing deep convection. *Geophysical Research Letters*, *51*(20), e2024GL110425. https://doi.org/10.1029/2024gl110425

Kurowski, M. J., Suselj, K., Grabowski, W. W., & Teixeira, J. (2018). Shallow-to-deep transition of continental moist convection: Cold pools, surface fluxes, and mesoscale organization. *Journal of the Atmospheric Sciences*, *75*(12), 4071–4090. https://doi.org/10.1175/jas-d-18-0031.1

Lunderman, S., Morzfeld, M., Glassmeier, F., & Feingold, G. (2020). Estimating parameters of the nonlinear cloud and rain equation from a large-eddy simulation. *Physica D: Nonlinear Phenomena*, *410*, 132500. https://doi.org/10.1016/j.physd.2020.132500

Malkus, J. S., & Scorer, R. S. (1955). The erosion of cumulus towers. *Journal of the Atmospheric Sciences*, *12*, 43–57.

Meyer, B., & Haerter, J. O. (2020). Mechanical forcing of convection by cold pools: Collisions and energy scaling. *Journal of Advances in Modeling Earth Systems*, *12*(11), e2020MS002281. https://doi.org/10.1029/2020ms002281

Moorthi, S., & Suarez, M. J. (1992). Relaxed Arakawa-Schubert. A parameterization of moist convection for general circulation models. *Monthly Weather Review*, *120*(6), 978–1002. https://doi.org/10.1175/1520-0493(1992)120<0978:rasapo>2.0.co;2

Morrison, H. (2017). An analytic description of the structure and evolution of growing deep cumulus updrafts. *Journal of the Atmospheric Sciences*, *74*(3), 809–834. https://doi.org/10.1175/jas-d-16-0234.1

Morrison, H., Peters, J. M., Chandrakar, K. K., & Sherwood, S. C. (2022). Influences of environmental relative humidity and horizontal scale of subcloud ascent on deep convective initiation. *Journal of the Atmospheric Sciences*, *79*(2), 337–359. https://doi.org/10.1175/jas-d-21-0056.1

Morrison, H., Peters, J. M., Varble, A. C., Hannah, W. M., & Giangrande, S. E. (2020). Thermal chains and entrainment in cumulus updrafts. Part I: Theoretical description. *Journal of the Atmospheric Sciences*, *77*(11), 3637–3660. https://doi.org/10.1175/jas-d-19-0243.1

Moser, D. H., & Lasher-Trapp, S. (2017). The influence of successive thermals on entrainment and dilution in a simulated cumulus congestus. *Journal of the Atmospheric Sciences*, *74*(2), 375–392. https://doi.org/10.1175/jas-d-16-0144.1

Neggers, R., & Griewank, P. J. (2021). A binomial stochastic framework for efficiently modeling discrete statistics of convective populations. *Journal of Advances in Modeling Earth Systems*, *13*(3), e2020MS002229. https://doi.org/10.1029/2020MS002229

Neggers, R., Stevens, B., & Neelin, J. D. (2006). A simple equilibrium model for shallow-cumulus-topped mixed layers. *Theoretical and Computational Fluid Dynamics*, *20*(5), 305–322. https://doi.org/10.1007/s00162-006-0030-1

Nelson, T. C., Marquis, J., Varble, A., & Friedrich, K. (2021). Radiosonde observations of environments supporting deep moist convection initiation during RELAMPAGO-CACTI. *Monthly Weather Review*, *149*(1), 289–309. https://doi.org/10.1175/mwr-d-20-0148.1

Nober, F. J., & Graf, H.-F. (2005). A new convective cloud field model based on principles of self-organisation. *Atmospheric Chemistry and Physics*, *5*(10), 2749–2759. https://doi.org/10.5194/acp-5-2749-2005

Pan, D.-M., & Randall, D. D. (1998). A cumulus parameterization with a prognostic closure. *Quarterly Journal of the Royal Meteorological Society*, *124*(547), 949–981. https://doi.org/10.1002/qj.49712454714

Peters, J. M., Hannah, W., & Morrison, H. (2019). The influence of vertical wind shear on moist thermals. *Journal of the Atmospheric Sciences*, *76*(6), 1645–1659. https://doi.org/10.1175/jas-d-18-0296.1

Peters, J. M., Morrison, H., Nelson, T. C., Marquis, J. N., Mulholland, J. P., & Nowotarski, C. J. (2022). The influence of shear on deep convection initiation. Part I: Theory. *Journal of the Atmospheric Sciences*, *79*(6), 1669–1690. https://doi.org/10.1175/jas-d-21-0145.1

Pinsky, M., Eytan, E., Koren, I., & Khain, A. (2022). Convective and turbulent motions in nonprecipitating Cu. Part II: LES simulated cloud represented by a starting plume. *Journal of the Atmospheric Sciences*, *79*(3), 793–813. https://doi.org/10.1175/jas-d-21-0137.1

Plant, R. (2010). A review of the theoretical basis for bulk mass flux convective parameterization. *Atmospheric Chemistry and Physics*, *10*(8), 3529–3544. https://doi.org/10.5194/acp-10-3529-2010

Plant, R., & Yano, J.-I. (2011). Comments on "An ensemble cumulus convection parameterization with explicit cloud treatment". *Journal of the Atmospheric Sciences*, *68*(7), 1541–1544. https://doi.org/10.1175/2011JAS3728.1

Powell, S. W. (2022). Criticality in the shallow-to-deep transition of simulated tropical marine convection. *Journal of the Atmospheric Sciences*, *79*(7), 1805–1819. https://doi.org/10.1175/jas-d-21-0155.1

Raymond, D. J., & Blyth, A. M. (1989). Precipitation development in a New Mexico thunderstorm. *Quarterly Journal of the Royal Meteorological Society*, *115*(490), 1397–1423. https://doi.org/10.1256/smsqj.49010

Rio, C., Del Genio, A. D., & Hourdin, F. (2019). Ongoing breakthroughs in convective parameterization. *Current Climate Change Reports*, *5*(2), 95–111. https://doi.org/10.1007/s40641-019-00127-w

Rio, C., Hourdin, F., Grandpeix, J.-Y., & Lafore, J.-P. (2009). Shifting the diurnal cycle of parameterized deep convection over land. *Geophysical Research Letters*, *36*(7), L07809. https://doi.org/10.1029/2008gl036779

Rochetin, N., Couvreux, F., Grandpeix, J.-Y., & Rio, C. (2014). Deep convection triggering by boundary layer thermals. Part I: LES analysis and stochastic triggering formulation. *Journal of the Atmospheric Sciences*, *71*(2), 496–514. https://doi.org/10.1175/jas-d-12-0336.1

Sakradzija, M., Seifert, A., & Heus, T. (2015). Fluctuations in a quasi-stationary shallow cumulus cloud ensemble. *Nonlinear Processes in Geophysics*, *22*(1), 65–85. https://doi.org/10.5194/npg-22-65-2015

Savre, J. (2023a). Outputs from new LBA simulations. Part I: Baseline case [Dataset]. *Zenodo*. https://doi.org/10.5281/zenodo.10409139

Savre, J. (2023b). Outputs from new LBA simulations. Part III: Suppressed cold pools [Dataset]. *Zenodo*. https://doi.org/10.5281/zenodo.10417550

Savre, J., & Craig, G. (2023). Fitting cumulus cloud size distributions from idealized cloud resolving model simulations. *Journal of Advances in Modeling Earth Systems*, *15*(5), e2022MS003360. https://doi.org/10.1029/2022ms003360

Savre, J., Ekman, A. M. L., & Svensson, G. (2014). Technical note: Introduction to MIMICA, a large-eddy simulation solver for cloudy planetary boundary layers. *Journal of Advances in Modeling Earth Systems*, *6*(3), 630–649. https://doi.org/10.1002/2013MS000292

Schiro, K. A., & Neelin, J. D. (2019). Deep convective organization, moisture vertical structure, and convective transition using deep-inflow mixing. *Journal of the Atmospheric Sciences*, *76*(4), 965–987. https://doi.org/10.1175/jas-d-18-0122.1

Schlemmer, L., & Hohenegger, C. (2014). The formation of wider and deeper clouds as a result of cold-pool dynamics. *Journal of the Atmospheric Sciences*, *71*(8), 2842–2858. https://doi.org/10.1175/jas-d-13-0170.1

Scorer, R., & Ludlam, F. (1953). Bubble theory of penetrative convection. *Quarterly Journal of the Royal Meteorological Society*, *79*(339), 94–103. https://doi.org/10.1002/qj.49707933908

Sherwood, S. C., Hernández-Deckers, D., Colin, M., & Robinson, F. (2013). Slippery thermals and the cumulus entrainment paradox. *Journal of the Atmospheric Sciences*, *70*(8), 2426–2442. https://doi.org/10.1175/jas-d-12-0220.1

Siebesma, A. P., Soares, P. M., & Teixeira, J. (2007). A combined eddy-diffusivity mass-flux approach for the convective boundary layer. *Journal of the Atmospheric Sciences*, *64*(4), 1230–1248. https://doi.org/10.1175/jas3888.1

Song, J., Song, F., Feng, Z., Leung, L. R., Li, C., & Wu, L. (2024). Realistic precipitation diurnal cycle in global convection-permitting models by resolving mesoscale convective systems. *Geophysical Research Letters*, *51*(13), e2024GL109945. https://doi.org/10.1029/2024gl109945

Strong, M. (2017). Time lapse of rising cumulus congestus III – Rising turrets with pileus. Retrieved from https://www.youtube.com/watch?v=2rHqVFu1m6w

Suselj, K., Kurowski, M. J., & Teixeira, J. (2019). A unified eddy-diffusivity/mass-flux approach for modeling atmospheric convection. *Journal of the Atmospheric Sciences*, *76*(8), 2505–2537. https://doi.org/10.1175/jas-d-18-0239.1

Takeuchi, Y. (1996). *Global dynamical properties of Lotka-Volterra systems*. World Scientific.

Tao, C., Xie, S., Ma, H.-Y., Bechtold, P., Cui, Z., Vaillancourt, P. A., et al. (2023). Diurnal cycle of precipitation over the tropics and central United States: Intercomparison of general circulation models. *Quarterly Journal of the Royal Meteorological Society*, *150*(759), 911–936. https://doi.org/10.1002/qj.4629

Teixeira, J., Suselj, K., & Kurowski, M. J. (2023). An introduction to the eddy–diffusivity/mass–flux (EDMF) approach: A unified turbulence and convection parameterization. In *Fast processes in large-scale atmospheric models* (pp. 271–282). American Geophysical Union (AGU). https://doi.org/10.1002/9781119529019.ch11

Tian, Y., Zhang, Y., Klein, S. A., & Schumacher, C. (2021). Interpreting the diurnal cycle of clouds and precipitation in the ARM GoAmazon observations: Shallow to deep convection transition. *Journal of Geophysical Research: Atmospheres*, *126*(5), e2020JD033766. https://doi.org/10.1029/2020jd033766

Torri, G., Kuang, Z., & Tian, Y. (2015). Mechanisms for convection triggering by cold pools. *Geophysical Research Letters*, *42*(6), 1943–1950. https://doi.org/10.1002/2015gl063227

Vogel, R., Albright, A. L., Vial, J., George, G., Stevens, B., & Bony, S. (2022). Strong cloud–circulation coupling explains weak trade cumulus feedback. *Nature*, *612*(7941), 696–700. https://doi.org/10.1038/s41586-022-05364-y

Vraciu, C. V. (2024). Generalized eddy-diffusivity mass-flux formulation for the parametrization of atmospheric convection and turbulence. *Quarterly Journal of the Royal Meteorological Society*, *150*(761), 2316–2337. https://doi.org/10.1002/qj.4711

Vraciu, C. V., Kruse, I. L., & Haerter, J. O. (2023). The role of passive cloud volumes in the transition from shallow to deep atmospheric convection. *Geophysical Research Letters*, *50*(23), e2023GL105996. https://doi.org/10.1029/2023gl105996

Wagner, T. M., & Graf, H.-F. (2010). An ensemble cumulus convection parameterization with explicit cloud treatment. *Journal of the Atmospheric Sciences*, *67*(12), 3854–3869. https://doi.org/10.1175/2010jas3485.1

Waite, M. L., & Khouider, B. (2010). The deepening of tropical convection by congestus preconditioning. *Journal of the Atmospheric Sciences*, *67*(8), 2601–2615. https://doi.org/10.1175/2010jas3357.1

Wu, C.-M., Stevens, B., & Arakawa, A. (2009). What controls the transition from shallow to deep convection? *Journal of the Atmospheric Sciences*, *66*(6), 1793–1806. https://doi.org/10.1175/2008jas2945.1

Yano, J.-I. (2014). Formulation structure of the mass-flux convection parameterization. *Dynamics of Atmospheres and Oceans*, *67*, 1–28. https://doi.org/10.1016/j.dynatmoce.2014.04.002

Yano, J.-I., Bister, M., Fuchs, Ž., Gerard, L., Phillips, V., Barkidija, S., & Piriou, J.-M. (2013). Phenomenology of convection-parameterization closure. *Atmospheric Chemistry and Physics*, *13*(8), 4111–4131. https://doi.org/10.5194/acp-13-4111-2013

Yano, J.-I., & Plant, R. (2012a). Finite departure from convective quasi-equilibrium: Periodic cycle and discharge–recharge mechanism. *Quarterly Journal of the Royal Meteorological Society*, *138*(664), 626–637. https://doi.org/10.1002/qj.957

Yano, J.-I., & Plant, R. S. (2012b). Interactions between shallow and deep convection under a finite departure from convective quasi equilibrium. *Journal of the Atmospheric Sciences*, *69*(12), 3463–3470. https://doi.org/10.1175/jas-d-12-0108.1

Zhao, M., & Austin, P. H. (2005). Life cycle of numerically simulated shallow cumulus clouds. Part II: Mixing dynamics. *Journal of the Atmospheric Sciences*, *62*(5), 1291–1310. https://doi.org/10.1175/jas3415.1

Zhuang, Y., Fu, R., Marengo, J. A., & Wang, H. (2017). Seasonal variation of shallow-to-deep convection transition and its link to the environmental conditions over the Central Amazon. *Journal of Geophysical Research: Atmospheres*, *122*(5), 2649–2666. https://doi.org/10.1002/2016jd025993